OPTICAL PROPERTIES OF NATIVE AND COAGULATED LAMB BRAIN TISSUES *in vitro* IN THE VISIBLE AND NEAR-INFRARED SPECTRAL RANGE

by

Korhan Özer

BS, in Electrical and Electronics Engineering Department,

Faculty of Engineering and Architecture,

Çukurova University, 2005

Submitted to the Institute of Biomedical Engineering

in partial fulfillment of the requirements

for the degree of

Master of Science

in

Biomedical Engineering

Bogaziçi University

June, 2005

OPTICAL PROPERTIES OF NATIVE AND COAGULATED LAMB BRAIN TISSUES *in vitro* IN THE VISIBLE AND NEAR-INFRARED SPECTRAL RANGE

APPROVED BY:

Assist. Prof. Dr. Murat Gülsoy..

(Thesis Supervisor)

Assoc. Prof. Dr. Hale Saybaşılı…………………………………..

Assist. Prof. Dr. Ata Akın…………………………………............

DATE OF APPROVAL: 17.06.2005

ACKNOWLEDGMENTS

I would like to thank my supervisor Assist. Prof. Murat Gülsoy, for not only his encouraging guidance, his kind academic support and most important for me, his confidence on me, but also, his ability about looking at events from different points of view that contributes me for exceeding difficulties during the time of this study.

I would like to thank Dr. Adnan Kurt for his contributions to make this study possible in Koç University Physics Department.

I would like to thank Assist. Prof. Ata Akın for being member for my thesis committee.

I would like to thank Assoc. Prof. Hale Saybaşılı for being a member for my thesis committee.

This study is a part of, 04X101 Boğaziçi University research project (M.G). I am deeply grateful to Boğaziçi University for their support.

And my friends. I would like to give my special thanks to research assistants Özgüncem Bozkulak and Haşim Özgür Tabakoğlu from biophotonics laboratory. I am very grateful to you for their academic support, kind friendship and most important, your patience. Thank you my friends.

Bora Büyüksaraç, thanks for your motivation support and friendship.

Hülya Özer, Turan Özer and Aslı Özer, my lovely family. This thesis is dedicated to you.

ABSTRACT

OPTICAL PROPERTIES OF NATIVE AND COAGULATED LAMB BRAIN TISSUES *in vitro* IN THE VISIBLE AND NEAR-INFRARED SPECTRAL RANGE

The aim of this study was to estimate optical properties (μ_a, μ_s, μ_t, μ_s', τ, α, g) of native and coagulated lamb brain tissues at three different temperatures (45°C, 60°C, 80°C) by means of measured data which formed due to light-tissue interactions in visible and near-infrared spectral range *in vitro*. For dosimetry planning and accurate surgery, information about optical properties of brain tissue is required. Since optical properties of brain tissue may change due to thermal effects during laser therapy, knowledge of optical properties of brain tissue coagulated at different temperatures should also be known for surgery.

During this experimental study, optical properties of cerebellum, brainstem, cortical (grey matter), and sub-cortical regions (white matter) of frontal lobe tissues of lamb brain were estimated. For estimation, optical measurement data were determined for either native or coagulated tissues. These measurement data were diffused transmittance, diffused reflectance, total reflectance and total transmittance.

In order to measure these data, an optical system was designed; light coming from a light source was focused on the monochromator which can emit light at desired single wavelength. Incoming light from exit slit of monochromator was focused on integrating sphere by means of optic lenses in order to get measured data from lock-in amplifier. Afterwards, data obtained from experiments were used to estimate optical properties of tissues by means of a software (CAL-g3) written in Biophotonics Laboratory of Boğazici University.

As a conclusion, it was stated that both μ_a and μ_s values of tissues increased as temperature increases. Also scattering coefficients decreased with the wavelength for all tissue types due to increase in Mie scattering.

Keywords: *Monochromator, tissue characterization, light-tissue interaction.*

ÖZET

DOĞAL VE KOAGÜLE OLMUŞ *in vitro* KUZU BEYİN DOKULARININ GÖRÜNÜR VE YAKIN KIZIL-ALTI ARALIKLARINDAKİ OPTİK ÖZELLİKLERİ.

Bu çalışmanın amacı, kasaptan alınan kuzu beyinlerinin *in vitro* olarak doğal halleri ile 45°C ,60°C, 80°C olmak üzere 3 farklı sıcaklıkta koagüle edilmiş hallerinin ışık dalga kuşağının görünür ışık ve yakın- kızılaltı aralıklarında ışıkla etkileşimleri sonucunda dokudaki etkilerinin ölçülerek, bu ölçümler doğrultusunda elde edilen veriler yardımıyla dokunun optik özelliklerinin hesaplanmasıdır. Doz planlanmasında ve doğru cerrahi uygulamalar için beyin dokusunun optik özelliklerinin bilinmesi gerekir. Ayrıca laser terapisi sırasında ortaya çıkan ısının da dokunun optik özelliklerini değiştirebileceği düşünüldüğünde, farklı sıcaklıklarda koagüle olmuş beyin dokusunun optik özellikleri de bilinmelidir.

Deneyler süresince kuzu beyninin beyincik, beyin sapı kısımları ile beynin ön lobunun kabuk(gri madde) ve kabukaltı (beyaz madde) dokuları deneylerde kullanıldı. Hesaplamalar için, dağınık iletim, dağınık yansıma, toplam yansıma ve dağınık yansıma değerleri hem doğal hem de koagüle olmuş deyin dokuları için ölçüldü.

Bu ölçüm verilerini elde etmek için optik düzenek hazırlandı.Işık kaynağından çıkan ışık optik tek dalga boyunda ışık yayabilen monokromatöre odaklandı. Monokromatörün çıkışından gelen ışık tümleşik kürenin üzerine, ölçümleri toplamak amacıyla optik lensler yardımıyla odaklandı. Deneylerden elde edilen ölçüm verileri Biophotonics labaratuvarında geliştirilen CAL-g3 yazılımı yardımıyla optik özelliklerin hesaplanmasında kullanıldı.

Sonuç olarak, dokuların sıcaklık değerleri arttırıldığında dokuların μ_a ve μ_s değerlerinin de arttığı gözlemlendi. Ayrıca Mie saçılmasındaki artıştan dolayı, dalga boyu arttıkça tüm dokularda saçılmada azalmalara rastlandı.

Anahtar Sözcükler: *Monokromatör, doku karakterizasyonu, ışık-doku etkileşimi* .

TABLE OF CONTENTS

LIST OF FIGURES

LIST OF TABLES

LIST OF ABBREVIATIONS

LASER	Light Amplification by Stimulated Emission of Radiation
Nd:YAG	Neodmium Yttrium Aluminum Garnet
Er:YAG	Erbium Yttrium Aluminum Garnet
KTP	Potassium titanium phosphate
CO_2	Carbondioxide
He-Ne	Helium-Neon
nm	Nanometer
mm	Milimeter
μm	Micrometer
ns	Nanosecond
W	Watt
CW	Continuous Wave
CNS	Central Nervous System
IAD	Inverse Adding Doubling
CAL-3g	Calculator-3g
NIR	Near Infrared
IR	Infrared
UV	Ultraviolet
DNA	Deoxyribonucleic acid
NA	Numerical Aperture
PLL	Phase Locked Loop
PSD	Phase Sensitive Detector

LIST OF SYMBOLS

μ_a	Absorption coefficient
μ_s	Scattering coefficient
μ_t	Total attenuation coefficient
τ	Penetration depth
α	Optical albedo
μ_s	Reduced scattering coefficient
λ	Wavelength
g	Anisotropy factor
n_1	Refraction index of medium 1
n_2	Refraction index of medium 2
k	Internal parameters other than concentration
c	Concentration
z	Distance
$L(r, s)$	Radiance of light at a position of 'r' travelling in a direction of unit vector 's'
dw	differential solid angle
$P(s, s')$	Phase function
T_t	Total transmittance
T_d	Diffused transmittance
T_c	Collimated transmittance
R_d	Diffused reflectance
R_t	Total reflectance
R_c	Collimated reflectance
I_0	Intensity of incident light
F	Focal point
f	Focal length
ๆ	Ratio of refractive indexes of two surfaces of the lens
R_1	Radius of first lens
R_2	Radius of second lens

1. INTRODUCTION

1.1 Light in Medicine

Recent years, light-based devices are widely used in medicine. The laser is one of the light-based devices which are used in medical applications. Since demonstration of first successful lasers in the early 1960's, they have become well established instruments in science, industry, communications and medicine. Lasers in medicine began with ophthalmology but nowadays the application area of medical lasers become widened [1].

Due to increasing use of light-based devices emitting energy at different wavelengths in medical applications, evaluation of optical properties of biological tissues become important [2]. When light interacts with biological tissue, it scatters from the tissue, it is absorbed in the tissue or transmitted through the tissue, and this is determined by optical properties of tissue. Information about effects of light on a tissue is very important for all kind of light applications.

Optical properties not only influence distribution and propagation of light in laser-irradiated medium, but also reveal light-tissue interaction mechanism inside biological tissue. For all diagnostic techniques, knowledge of optical properties of tissues is of basic importance for a proper choice of operational wavelength [2], this choice provides surgeon to differentiate the region of interest and surrounding healthy tissue. Optical properties of tissues estimated due to light-tissue interactions, are not only important to choose the operational wavelength, but also essential for dosimetry in cancer treatments utilizing laser light, photodynamic tumors therapy and photo-thermal treatments [2]. Because of that, the laser type and its application power, exposure time and energy density used in neurosurgery, are all chosen due to optical properties of tissues.

Besides increasing use of light as a therapeutic tool, the propagation of it in tissue and transformation of thermal energy due to absorption of light is governed by optical tissue properties [2].

1.2   Motivation

As mentioned above, for successful dosimetry planning and for accurate laser surgery, information about the optical properties of desired native and coagulated brain tissue are required [3]. In view of estimating laser energy distribution throughout the biological tissues, these optical properties are crucial parameters.

The aim of this study is to estimate optical properties of cerebellar tissue, brainstem, cortical and subcortical regions of native and coagulated brain tissue samples. Coagulation was done at different temperatures (45°C, 60°C, 80°C). Optical measurements were done at wavelengths which are chosen from the visible and near infrared range of light spectrum.

By using experimental setup, measured data were acquired due to light-tissue interaction. These measured data are total transmittance (T_t), total reflectance (R_t), diffused transmittance (T_d) and diffused reflectance (R_d). These data were obtained for 8 different wavelengths (488, 514, 532, 633, 780, 810, 880 and 905-nm). Afterwards, data obtained from experiments were used to estimate absorption coefficient (μ_a), scattering coefficient (μ_s), reduced scattering coefficient (μ_s'), penetration depth (τ), total attenuation coefficient (μ_t) and anisotropy factor (g) of tissues by means of software CAL-g3.

Optical properties of brain tissue may change due to thermal effect of laser during the therapy, heat-induced changes of the optical properties in tissue should be determined. Thus, optical properties of coagulated tissues at 45°C, 60°C and 80°C were also estimated and compared with reported literature values.

1.3   Outline

In Chapter 2, theory of light transport and light-tissue interaction, optical properties of a biological tissues and the anatomy of brain were explained as well as monochromator principles.

Chapter 3 gives information about the optical system which is set in laboratory. In this chapter, measurement method and software developed in Biophotonics laboratory are also explained.

Results that are taken from the experimental setup are calculated and desired optical properties are estimated in chapter 4. In chapter 5, both analysis of optical properties and discussion were done.

In chapter 6, general conclusion and contribution of this study for further scientific works can be found.

2. THEORY

2.1 Optical properties of Biological tissues

2.1.1 Theory of Light

Biological tissues are optically inhomogeneous and absorbing media whose refractive index is higher than that of air [4]. Thus, some part of light coming from the source is reflected backward (Fresnel reflection), when the other part goes deep inside the tissue. Multiple scattering and absorption events occur during this penetration, and the light attenuates as it travels. Cellular organelles such as mitochondria are the main scattering substances in various tissues [4, 5].
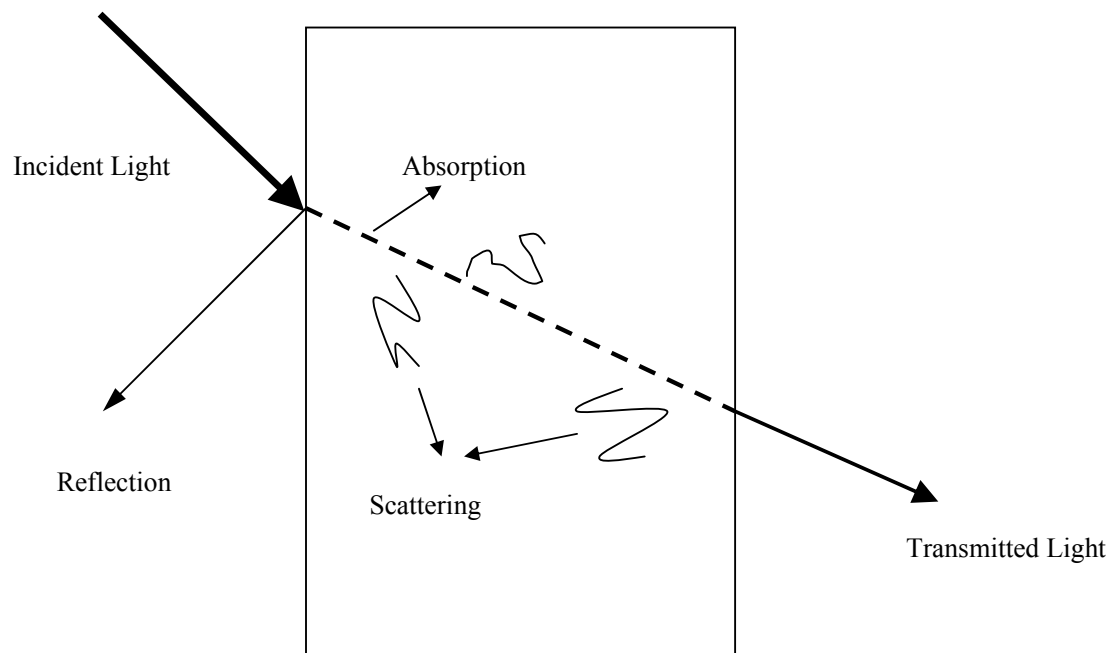
Figure 2.1 Propagation of Light in tissue in case of light-tissue interaction.

Refraction usually occurs when the reflecting surface separates two media of different indices of refraction. It originates from a change in speed of the light wave [4].
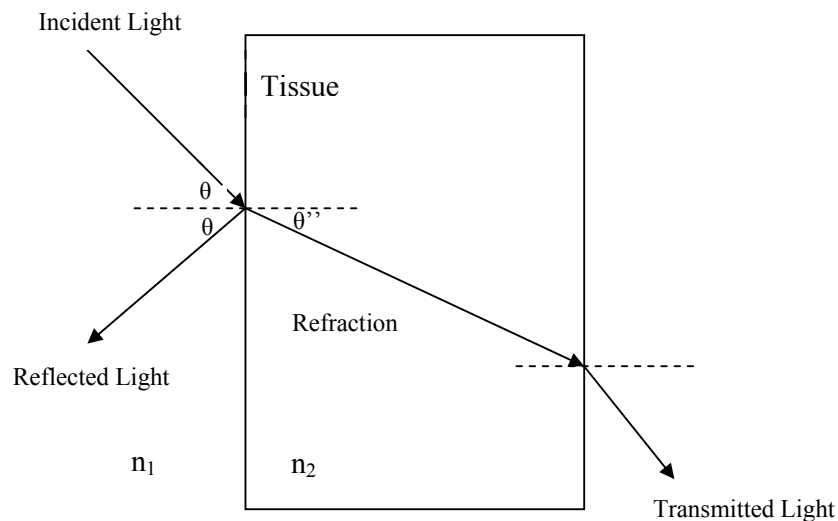
Figure 2.2 Geometry of reflection and refraction.

n_1 is the refraction index of the first media and n_2 is the refraction index of second media.(Figure 2.2). Then

$$n_1 \times \sin\theta = n_2 \times \sin\theta^{"}$$ (2.1)

This rule is called Snell's law. If sine(θ) > n_2 / n_1, then refraction does not occur. This condition is also called total reflection.

During absorption, intensity of electromagnetic wave is attenuated through the medium. It is a measure of the rate of decrease in the intensity of electromagnetic radiation (as light) as it passes through a given substance. Chromophores are main absorber substances in a broad sense and they mediate absorption in tissue. Different chromophores have different absorption spectra. The absorbance of a medium is defined as the ratio of absorbed and incident intensities [4]. Absorbed light is converted into heat or radiated in the form of fluorescence [5]. Absorption ability at a specific wavelength radiation is related to many factors: Thickness of the absorbing medium, tissue type, an

electronic constitution of medium's atoms and internal parameters (such as concentration of water and temperature) [4, 5]. Also concentration and absorption characteristics of tissue chromophores such as DNA, water, pigments and intracellular molecules together affect the absorption ability [6]. In biological tissues, absorption is mainly caused by either water molecules or macromolecules such as pigments (pigment of hemoglobin, myoglobin, melanin and bilirubin) and proteins [7]. Change of absorption coefficients of some molecules in human body due to wavelength is shown below (Figure 2.3).
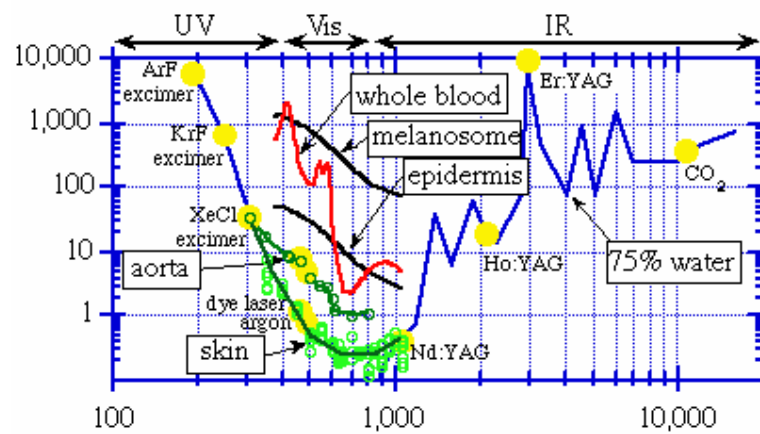
Figure 2.3 Change of absorption coefficient of some molecules in human body due to the wavelength of electromagnetic radiation [8]. y axis shows absorption coefficient values (cm^{-1}) and x axis shows wavelength (nm).

In IR region absorption is attributed to water molecules but proteins and pigments mainly absorb light in the UV and visible range [8]. In ultraviolet, the absorption increases with shorter wavelengths due to protein, DNA and other molecules. In infrared, the absorption increases with longer wavelengths due to tissue water content. In the red to near-infrared (NIR), absorption is minimal. This region is called the diagnostic or therapeutic window [8].

Two laws are very important on determination of effects of thickness and concentration on absorption. These are called Beer's law and Lambert's law:

$$I(z) = I_0 \times e^{-\mu_a z} \tag{2.2}$$

And,

$$I(z)=I_0 \times e^{-k' \times c \times z}$$

(2.3)

In these formulas, 'z' is the optical axis and I (z) is the intensity at a distance 'z'. I_0 is the incident light intensity, μ_a is the absorption coefficient of the medium, k' is internal parameters other than concentration and 'c' is concentration [4, 5, 8]. So these two laws describe the same behaviour of the absorption, they also known as Lambert- Beer's law:

$$z = \frac{1}{\mu_a} \times \left[\ln \left(\frac{I_0}{I(z)} \right) \right]$$

(2.4)

Scattering of light occurs as a direct result of the interaction of light with random variations in refractive index or small particles in the medium, resulting in a dispersion of the light in all directions. In particular, scattering results from microscopic and macroscopic constituents such as cellular membranes or refractive index mismatching between intra and extra-cellular fluids, mitochondria, ribosome, fat, globules and collagen fibrils within the extra cellular matrix [7, 9]. Combined attributes of low absorption and high scattering in tissue allow light to penetrate deeper within tissue, approximately 1-10 cm enabling non-invasive extraction of deep tissue information.

2.1.2 Tissue and Turbid Media

Optical properties are obtained by converting measurements of observable quantities into parameters which characterize light propagation in tissue [10]. Quantitative knowledge of light distribution in biological medium can be achieved from the solution of radiative transfer equation provided that accurate values of basic optical properties of the medium are available. In case of laser energy transport, transfer theory is preferred to Maxwell's equations because of imhomogenity of biological tissue. According to transport theory, the radiance L(r, s) of light at position 'r' travelling in a direction of unit vector 's' is decreased by absorption and scattering but it is increased by light that is scattered from s' directions into the direction 's'. Formulation of transport equation assumes that each scattering particle is sufficiently distant from its neighbours preventing

interactions between successive scattering effects [11]. Radiative transport equation which describes the light interaction is [12]:

$$s \times \nabla L(r,s) = -\mu_t \times L(r,s) + \int_{4\pi} p(s,s') \times L(r,s') \times dw \qquad (2.5)$$

Where μ_t is attenuation coefficient and dw is the differential solid angle in the direction of s' and p(s, s') is the phase function.

In most tissues, either scattering or absorption occurs at the same time. This type of media is called turbid media. Their total attenuation coefficient can be expressed by

$$\mu_t = \mu_a + \mu_s \qquad (2.6)$$

Where μ_a is absorption coefficient and μ_s is scattering coefficient. In turbid media mean free optical paths (penetration depth) of incident photons are thus determined by [4, 5, 12],

$$\tau = \frac{1}{\mu_t} \qquad (2.7)$$

$$\mu_s' = \mu_s \times (1-g) \qquad (2.8)$$

μ_s', is called reduced scattering coefficient.

In some cases, scattering or absorption coefficient can be neglected. Another important parameter is called optical albedo. Albedo α is a dimensionless parameter defined as the ratio of scattering to the sum of scattering and absorption [11].

$$\alpha = \frac{\mu_s}{\mu_t} \qquad (2.9)$$

If $\alpha=0$, attenuation is exclusively due to absorption but if $\alpha=1$, only scattering occurs [4].

Anisotropy can be characterized by average cosine of the scattering angle [10]. 'g' approaches -1,0,1 that corresponds highly backward, isotropic, and forward scattering respectively [4, 10, 12].

2.2   Anatomy of Brain

Central nervous system (CNS) consisting of the brain and spinal cord, receives input from sensory neurons and directs the activity of motor neurons that stimulate the activity of muscles and glands.

CNS is composed of grey and white matter. Grey matter is on the cortex (surface of brain) and deeper within the brain in aggregations known nuclei. It is composed of neuron cell bodies and dendrites. White matter consists of axon tracts under the cortex and surrounds nuclei [13].

2.2.1   Brain Regions

Brainstem is the lower extension of the brain (Figure 2.4). It connects to the spinal cord. Neurological functions located in the brainstem include those for survival (breathing, digestion, heart rate, blood pressure) and for arousal (being awake and alert). Most of the cranial nerves come from the brainstem. Brainstem is the pathway for all fiber tracts passing up and down from peripheral nerves and spinal cord to the highest parts of the brain [14].
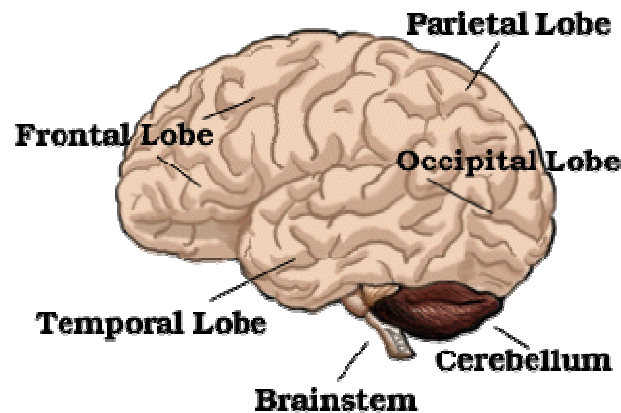
Figure 2.4 Anatomical structure of the brain [13].

Cerebellar tissue is the main structure in the hindbrain situated at the base of the brain, at the top of the spinal cord (Figure 2.4). Cerebellar tissue controls our balance and postural stability, and is involved in motor coordination. Also it is involved performance and improvement of learned motor skills. Damage may result in ataxia which is a problem of muscle coordination. This can interfere with a person's ability to walk, talk, eat, and to perform other self care tasks. It is also thought that cerebellar tissue involves the processing speech and language [14].

Frontal Lobes are situated at the "front" of the cortex, behind the forehead. They are the largest of the lobes in the cerebrum and may be thought of as the "highest" part of our brain. It is responsible for reasoning, planning, attention, some aspects of language. It is also involved in planning, organizing, problem solving, selective attention, personality and a variety of "higher cognitive functions" including behaviour and emotions [14]. The anterior (front) portion of the frontal lobe is called the prefrontal cortex. It is very important for the "higher cognitive functions" and the determination of the personality. The posterior (back) of the frontal lobe consists of the premotor and motor areas. Nerve cells that produce movement are located in the motor areas. The premotor areas serve to modify movements [14].

2.3   Effects of Laser - Tissue Interaction

The interaction of a laser light with tissue depends on exposure time, the wavelength of the radiation itself, as well as the optical properties of the tissue which is determined by the structure, water content and blood circulation, conductivity, heat capacity and density of tissue [4]. There are four major classes of laser interaction with neural tissue. These are photothermal, photochemical, photodisruptive and photoablative mechanisms.   If laser energy and exposure time are low, effects are photochemical. Another effect is photo thermal, which forms due to energy conversion of light into heat. Photomechanical effect is formed due to rapid tissue heating with very short and high energy pulses resulting in increased local pressure with explosion and tissue photoablation (Figure 2.5) [15].
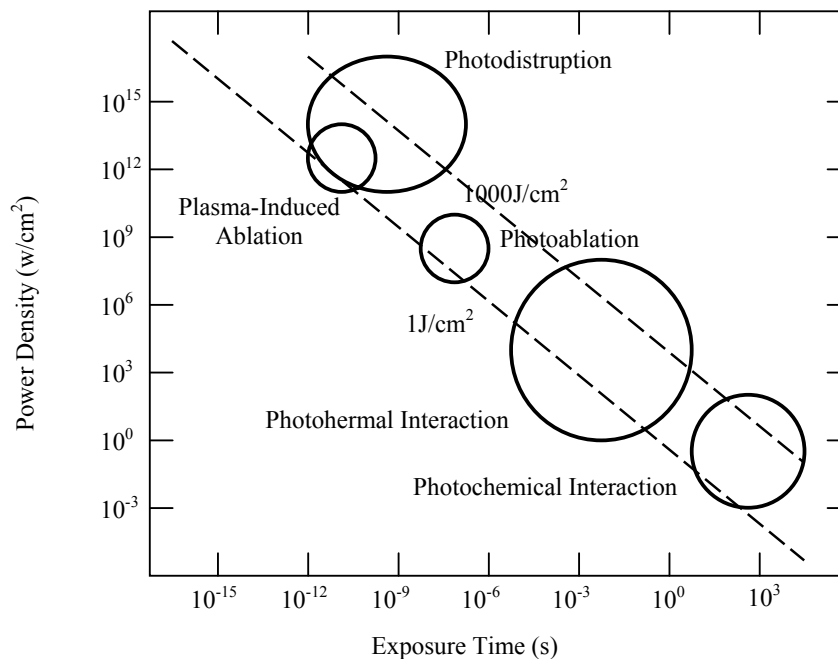
Figure 2.5 Classification of laser-tissue interaction due to exposure time and energy density [4].

Laser-tissue interaction effects between 50°C -100°C are called haemostasis (water evaporation, protein denaturising, tissue retraction). Between 43°C-45°C cell death begins (Hyperthermia).   Between 50°C and 60°C the enzymatic activities are reduced by denaturation of the macromolecules (like proteins, collagens, lipids, haemoglobin) that is at the basis of the coagulation process. Increase in temperature destroys the organisation

of macromolecular chains. Thermal denaturation of the intercellular proteins disrupts tissues' regular structure. Vaporization process begins at 100°C, mainly due to the heating of the free water in the tissues [16].

Light fluence distribution in tissue depends on optical properties of tissues. Absorption and scattering coefficients, that affect penetration of light into neural tissues, are wavelength dependent. Because of that, type and total power of laser used in neurosurgery, exposure time and energy density are all chosen due to optical properties of tissues which are evaluated before. Inhomogenity in blood and water concentration and their different absorption and scattering windows in light spectrum, protein and lipid arrangement in normal and abnormal tissues causes requirement of knowledge about their optical properties in order to choose precise and accurate laser type during operation. For example, penetration of CO_2 laser into the tissue never exceeds 300μm while penetration depth of Nd:YAG laser is between 2 and 3,5mm. Since, Nd:YAG is used in order to emit energy into deeper tissues and wider areas. Heating of tissue by this laser also slower compared to CO_2 laser. It is also stated that, chromophores and their absorption spectra are also very important in heating of tissue. For example as seen from (Figure 2.3), lasers emitting at water absorption peaks are absorbed by neural tissues and give local effects such as vaporization with minimal penetration into tissue. Heat production depends on optical penetration, blood flow and thermal conductivity as well as specific heat of tissue [4, 6, 17].

2.3.1 Lasers in Neurosurgery

Surgical lasers appear to offer a less traumatic and more haemostatic technique for the ablation of both tumour and neural tissues. Recent years, not only biological effects from interaction of laser energy and neural tissue, but also non-touch technique avoiding mechanical trauma make laser one of the popular surgical instrument in neurology [13]. There are different types of lasers which are used in medicine especially in neurosurgery.

1. Solid state lasers (Ruby laser, Nd:YAG, Er:YAG,)
2. Dye lasers

3. Gas lasers (CO_2, excimer laser, ion lasers)

4. Semiconductor lasers.

These lasers can be classified into two groups. First three are named as conventional lasers and last one, diode lasers, are very prospective technique in neurosurgery in recent years.

First reported laser experiment which is used in neurosurgery is done by Rosomoff and Carroll in 1966. Between 1965 and 1970 ruby lasers and argon lasers are used on the central nervous systems of different subjects such as rats, dogs and pigs [15]. They used ruby laser irradiation for several brain tumours. Use of different lasers, as a neurosurgical instrument has been achieved by Stelar in 1963. He totally vaporized a recurrent glioma with a CO_2 laser [6].

CO_2 laser, emits between 9400-10600nm. Penetration depth of this laser is very small (less than 0.2mm). Also it is less haemostatic than other lasers. Light conversion into heat occurs very fast within small volume of tissue. One of absorption peaks of water corresponds to spectral value of this laser. This rapid increasing local heat level makes this laser good cutting tool at CW power between 20-30W. The advantages of CO_2 laser surgery for excision of gliomas, poorly accessible deep tumours, basal extra-axial lesions of brain and spinal cord [6]. Since CO_2 laser emits in far infrared region, it is used with helium-neon laser to provide a visible aiming beam. He-Ne beam is aligned perfectly with CO_2 beam allowing surgeon to direct the energy accurately [17].

Nd:YAG laser(1.06μm), is a solid state laser that uses a crystal of yttrium aluminium garnet doped with a trace quantity of the earth neodymium, which is actual lasing medium, it is selectively absorbed by haemoglobin with a blood which makes it applicable for neurovascular surgery. In contrary to CO_2 laser, Nd:YAG laser has low water absorption properties and it can be used fiber guided which makes it easier to use. Due to low water absorption properties, Nd:YAG laser can also easily penetrates into spinal cord and brain. Due to brain penetration by scattering and head conduction, it produces deep tissue heating and necrosis [15]. Due to lack of precision and control difficulties related to heating effects it was stated that Nd:YAG laser is not applicable to

neural tissue operations. Nd:YAG laser was also found to be beneficial in softening fibrous or calcified tumours by Takeuchi *et al* [17].

KTP laser (532-nm) is a frequency doubled Nd:YAG laser through a potassium titany phosphate crystal. It was supposed that KTP is absorbed by pigments but not by water. This absorption property of KTP makes it very useful in coagulation applications [15].

2.3.2   Diode Lasers in Neurosurgery

Conventional lasers are widely used in neurosurgery for removal of tumours as well as vascular malformations. But their bulk and necessary setup including gas and water equipment, power supply, their price and limited movement capability are disadvantages of conventional lasers. Thus, due to low price, available small size, portability and reliability, high power diode lasers are much more preferred by surgeons in recent days [15].

First surgical diode laser used in neurosurgery is 805nm diode laser. Despite low absorption by water; this wavelength is highly absorbed by haemoglobin and melanin [16]. This laser penetrates into deep tissue due to chromophore concentration. Thus it is very dangerous. High power diode lasers can be used in contact mode or non-contact mode. But Devaux et al stated their researches on 30 cases and eventually they found that 805-nm high power diode causes some problems such as carbonization in contact mode applications [16]. Diode laser was found to have more local effect due to high absorption and low penetration depth.

Another high power diode laser model is 980nm diode laser. Researches stated that this laser could be beneficial neurosurgical device [18]. Gulsoy *et al* reported that CW laser energy delivered at 980-nm vaporized tissue with limited coagulation zone around target area and carbonization was not observed. Limited coagulation was found implying minimal thermal damage to surrounding tissues in subcortical area of the rat brain [18]. These results are related to one of the absorption peaks of water at 980-nm. (Figure 2.3)

3. METHOD

As mentioned before, purpose of this thesis project is to estimate optical properties of brain tissues. Thus, an experimental setup was prepared for optical measurements such as Td, Tt, Rd, Rt which were required for determination of optical properties. After these values were acquired, software called CAL-g3 has been used for modelling which finally gave desired tissue characterization values. Flow chart of method which was used for tissue characterization in this project is shown (Figure 3.1):
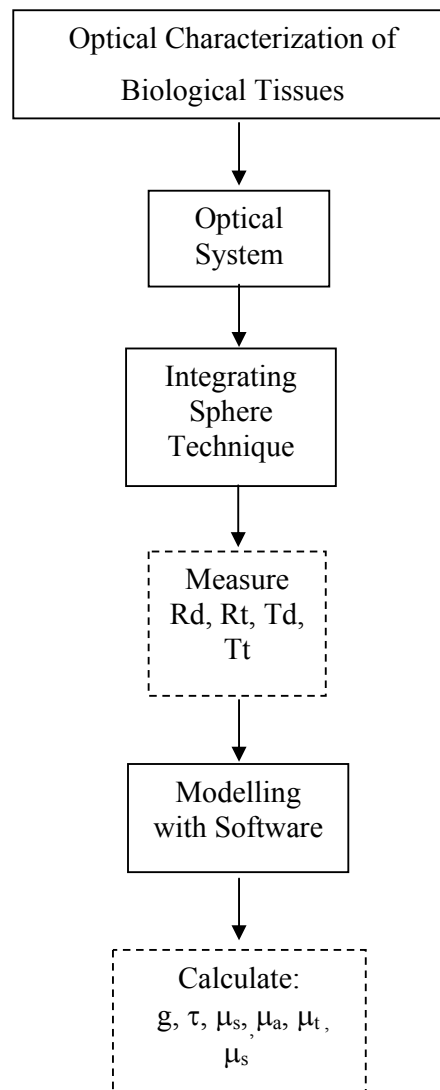
Figure 3.1 Flow chart of optical characterization of tissues.

3.1   Measurement of Optical Properties of Biological Tissues

3.1.1   Experimental Setup and Lens System Design

Lens is defined as an optical element consisting of two or more refractive surfaces that share a common axis. Space between two refractive surfaces of the lens is filled with either air or any appropriate liquid.

When light comes through lens, it is refracted by both surfaces of the lens. Single point to which light rays are converging is called focal point. The distance, f, from the lens to the focal point F is the focal length. Each lens and mirror has its own focal length, which is its defining characteristic. For a thin lens in the air,

$$\frac{1}{f} = (\eta - 1) \times \left[\frac{1}{R_1} + \frac{1}{R_2} \right] \tag{3.1}$$

Where R_1 and R_2 are radii of curvature of first and second surfaces of lens, and η is ratio of refractive indexes of two surfaces of the lens (Figure 3.2). This formula also called spherical lens maker's equation [19].

Amount of light that is collected by lens is defined by the aperture (A) of lens. If the aperture is reduced, then rays which would strike the edges of the lens from entering. are blocked. If the aperture is reduced, then amount of light passing through optical system will also be reduced [20]. This is a trade off that is common in optical design. As apertures are made smaller, field of view of system also became smaller and less light enter the system, which results smaller aberrations.

Lens Aperture (A)

Object Plane

Cone Half Angle

F

R$_2$

R$_1$

Chief Ray

f

Optical Axis
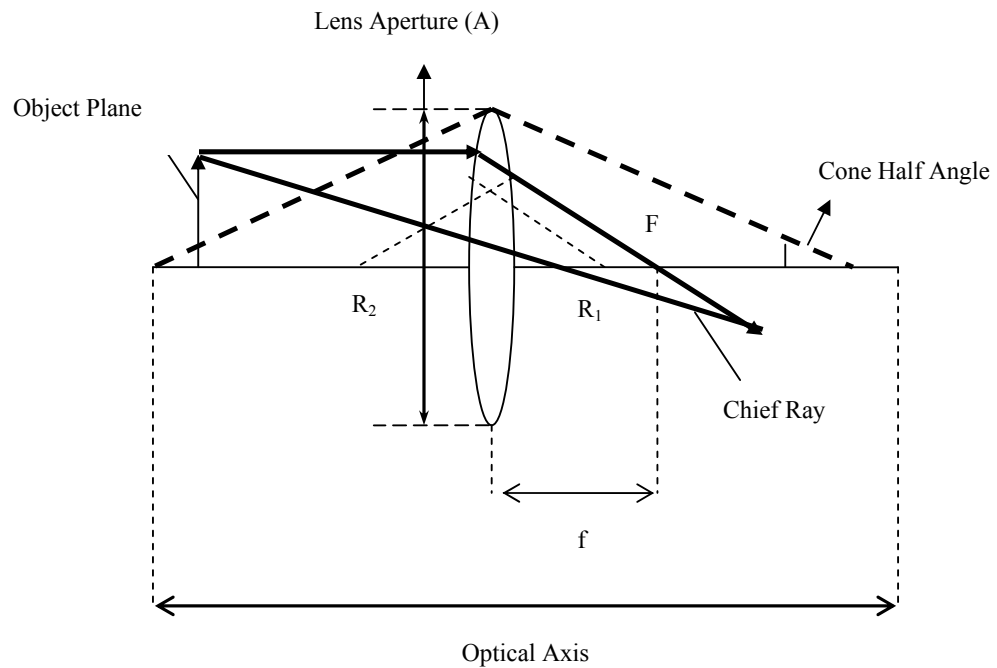
Figure 3.2 Characteristic properties of simple lens system.

In this study two types of lenses were used:

- Biconvex lenses
- Aspherical lens

Biconvex lenses have same principals like the one discussed above. Aspherical lenses are different from biconvex lenses. These types of lenses have some advantages over biconvex simple lenses. In spherical lens generally it is impossible to converge parallel rays at one point. Since many lenses are combined to correct it, there were limits in achieving higher performance of a large-aperture lens and compactness of lens. But these limits can be broken if you use the aspherical lens with ideal curved surface which can gather rays at one point. In other words, in spherical lens, rays coming from the lens periphery form the image before the ideal focal point. For this reason, the spherical aberration occurs at the centre portion of the image formed. But with aspherical lens, on the contrary, even the rays coming from the lens periphery agree on the focal point, thus forming a sharp image [21].

In this study, two different optical systems were designed for each measurement systems (transmittance measurements and reflectance measurements) by using lens systems (Figure 3.3, 3.4). System between light source and monochromator is same for both measurements whereas system between monochromator exit and sphere is different for each measurement. In figure 3.3, sample was placed on front port of integrating sphere in order to get total transmittance and diffused transmittance values. In order to get reflectance measurements, tissue sample was placed on back port of integrating sphere (Figure 3.4). To focus incoming light onto back port of sphere, one more lens (L7) was used. These values were detected by detector which was connected between sphere side port and lock-in amplifier. System details will be explained in following chapters.

Technical properties of these lenses are shown (Table 3.1).

Table 3.1

Characteristics of lenses.

Lens Number	Aperture (mm)	Focal Length (mm)	Lens Type
L1	25,4	25,4	Biconvex
L2	25,4	25,4	Biconvex
L3	25,4	50	Biconvex
L4	25,4	25,4	Biconvex
L5	25,4	25,4	Biconvex
L6	21	18	Aspheric
L7	25,4	50	Biconvex
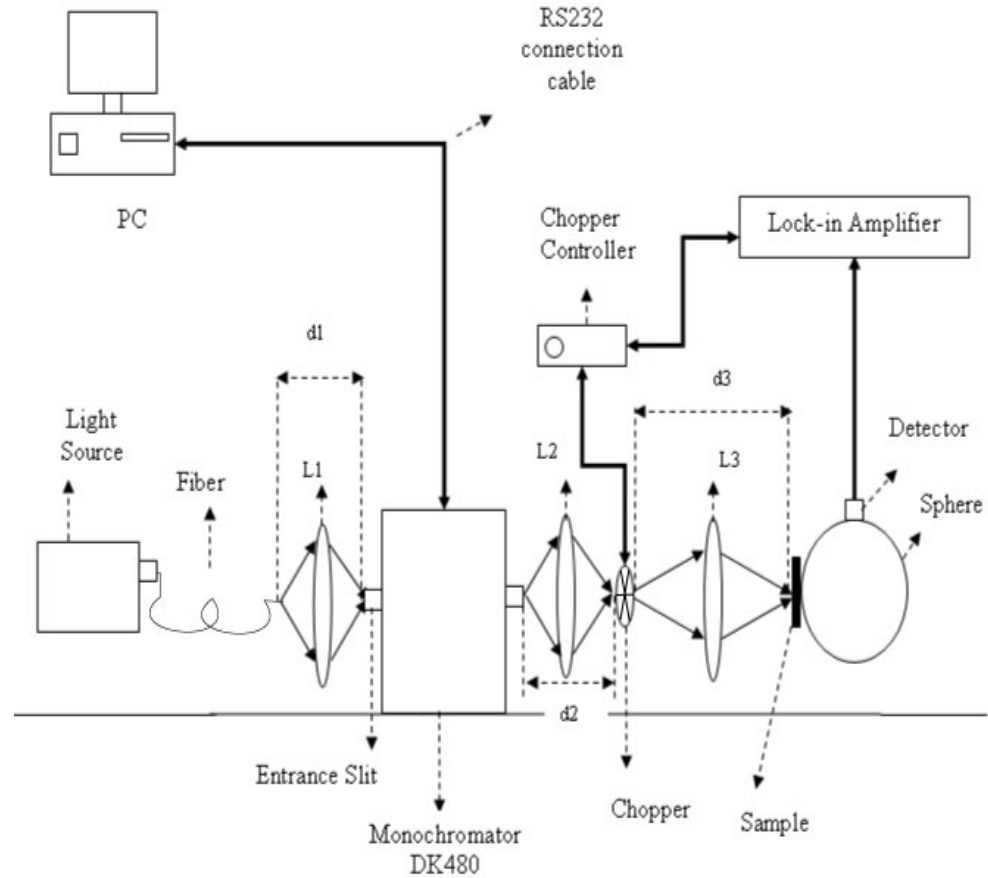
Figure 3.3 Experimental setup and optical design for transmittance measurements. Sample is placed on front port of integrating sphere to get transmittance measurements. Lens L1 is used to focus light coming from liquid fiber guide on monochromator entrance slit. Lens L2 is used to focus light coming from monochromator on external grids of chopper. Lens L3 is used to focus light that is chopped, on front port of integrating sphere. Data is sensed by detector that is connected to sphere and measured data is acquired from lock in amplifier. PC is used to control monochromator.
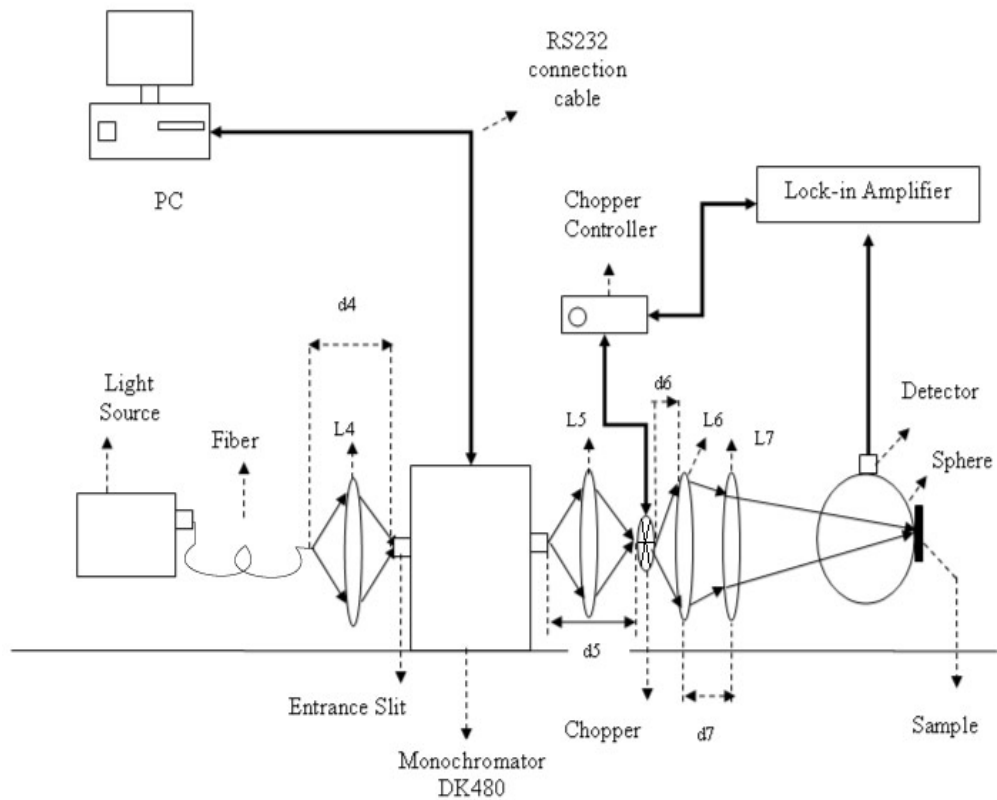
Figure 3.4 Experimental setup and optical design for reflectance measurements. Sample is placed on back port of integrating sphere to get reflectance measurements. Lens L4 is used to focus light coming from liquid fiber guide on monochromator entrance slit. Lens L5 is used to focus light coming from monochromator on external grids of chopper. Lens L6 and lens L7 are used to focus light that is chopped, on back port of integrating sphere. Data is sensed by detector that is connected to sphere and measured data is acquired from lock in amplifier. PC is used to control monochromator.

Distance values are calculated due to lens characteristics either focus maximum light from light source into monochromator or focus the light came from exit slit of monochromator into the integrating sphere. These values are shown below (Table 3.2).

Table 3.2

Lens Distance values in experimental setup.

Distance Number	Distance Value (mm)
d1	101,6
d2	101,6
d3	100
d4	101,6
d5	101,6
d6	18
d7	80

3.1.2   Light Source and Monochromator Principles

In this experimental setup, light source (Milla Luce M1000, Stocker Yale) is used. Before experiments, in order to get maximum light, photo detector (AD130, Spectral Products, Florida, USA) is used to measure light intensity of light (Figure 3.5).

Since light that is emitted from optic illuminator is not collimated enough, scattering is too high to focus it on the entrance slit of monochromator. A liquid fibre guide is mounted on the exit slit of light source. This liquid fibre guide can carry light nearer to monochromator with minimum scattering. By using lens system between fiber and monochromator, this unfocused light is collected on entrance slit of monochromator (Figure 3.6). All optical systems that are used in experimental setup are used to get minimum light dissipation.
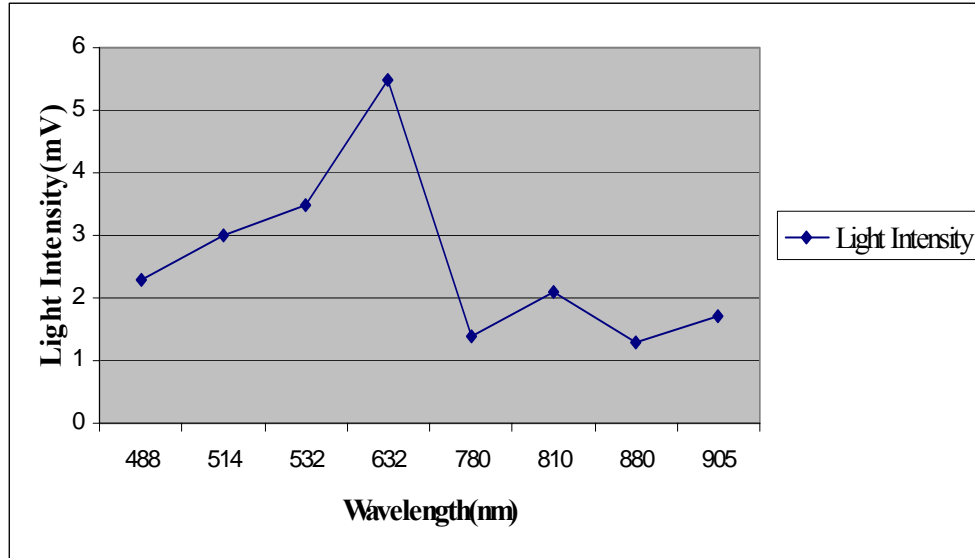
Figure 3.5 Light intensity of Milla LuceM1000 light source versus wavelength.

Monochromator is a spectrometer that capable of measuring single wavelength which can be scanned in a wide range of spectrum (Figure 3.7). In this figure the light coming from the light source is focused on entrance slit and directed by turning mirror (M1) to the collimating mirror(C). Then this focused light beam is directed to the grating (G) and due to the command which is coming from the controller , this grating rotates and get position in order to diffracts and reflects desired wavelength. Then this particular wavelength is directed to the focusing mirror (F) which is designed to focus beam to exit slit via second turning mirror (M2) [22].

In this project, DK480 (Digikröm 480 Spectral Products, Florida, USA) monochromator is used in order to get desired wavelength from the exit slit which is than focused on integrating sphere. Software is used to adjust slit thicknesses. Entrance and exit slit thicknesses are adjusted at 2000μm by using product software. Wavelength resolution of DK480 is reduced as entrance slit thickness increases but this is a trade off. In order to get maximum light, entrance slit thickness should be wide enough. Wavelength resolution is not important if near wavelengths are not desired like in this experimental study.

Light Source   Liquid Fibre guide   Monochromator
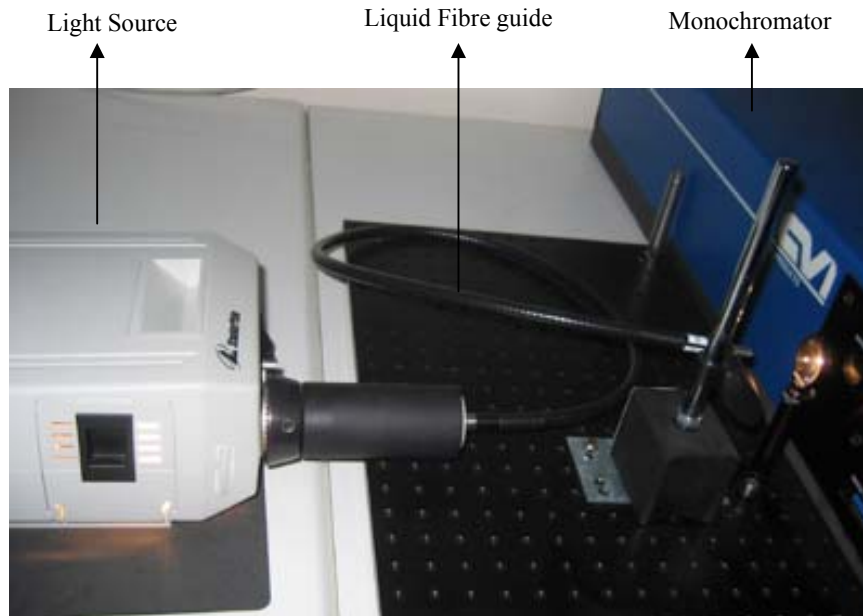
Figure 3.6 Optical setup between light source and monochromator. Liquid fibre guide is used to carry light more collimated near monochromator entrance slit. Lens is used to focus light onto the entrance slit of monochromator.

After light pass through DK480, desired wavelength can be acquired from exit slit by means of gratings inside the monochromator. In other words, wavelength range of monochromator is controlled by rotation of gratings. Grating adjustment and wavelength choice are controlled by using different software called Dk-Abi which was developed in Koç University (Figure 3.8).

Generally, one grating is not enough to get the desired wavelength. For example, monochromator DK480 which is used in this experimental setup in biophotonics laboratory has three gratings to get maximum efficiency in light quality for different wavelength ranges (Table 3.3). Since experiments were made in visible and near infrared range of light spectrum, second grating of monochromator is used.
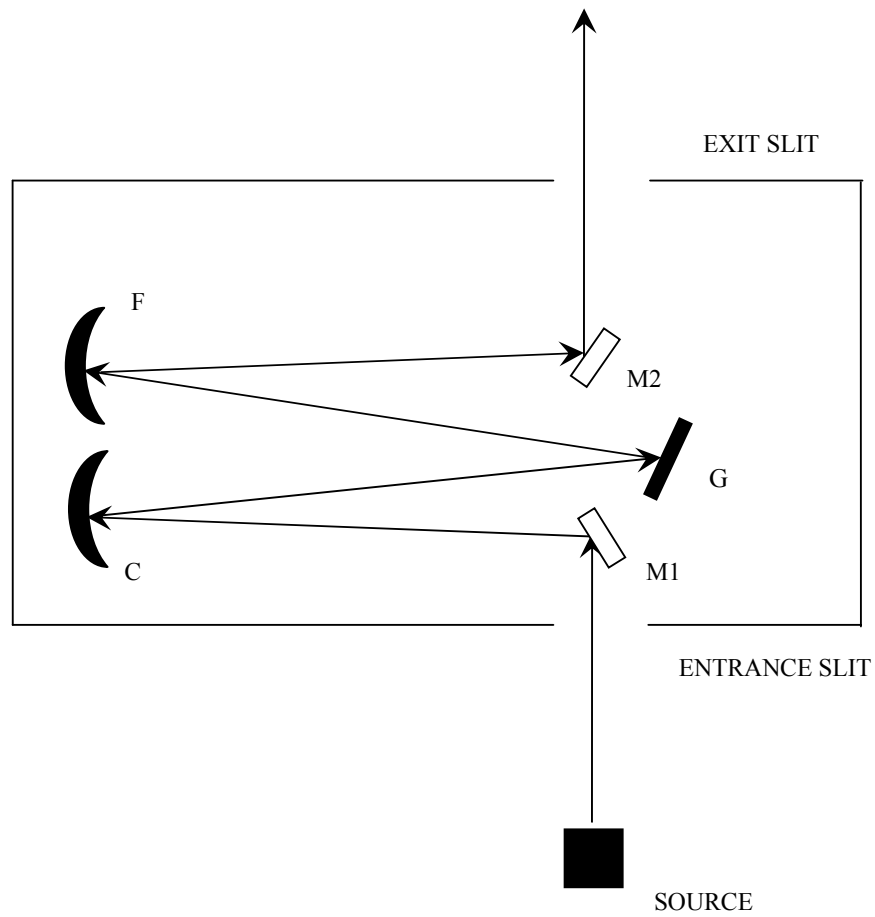
Figure 3.7 Monochromator DK480 principles [22].
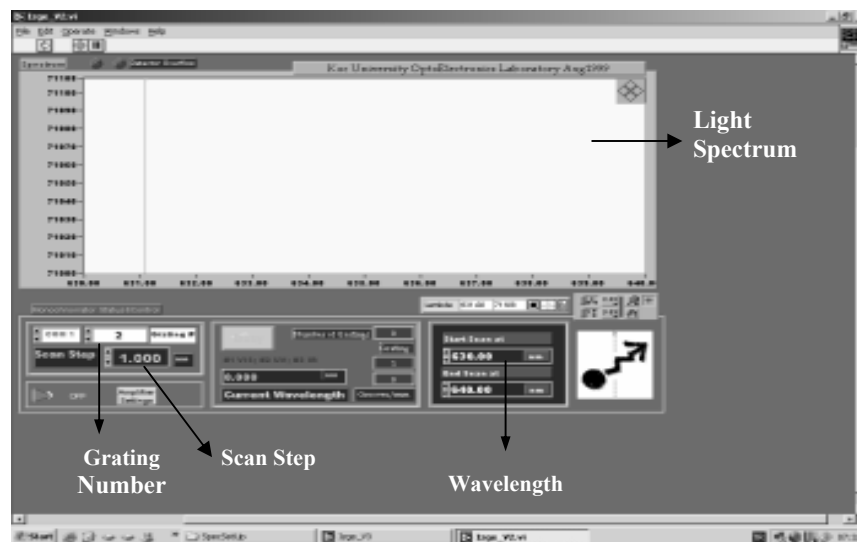
Figure 3.8 Dk-Abi software interfaces.

Generally, one grating is not enough to get the desired wavelength. For example, monochromator DK480 which is used in this experimental setup in biophotonics laboratory has three gratings to get maximum efficiency in light quality for different wavelength ranges (Table 3.3). Since experiments were made in visible and near infrared range of light spectrum, second grating of monochromator is used.

Table 3.3

Grating wavelength ranges in DK480 monochromator.

Grating	Wavelength (nm)
1	200-750
2	310-1100
3	1500-4500

Parameters such as spectral resolution, wavelength accuracy and precision could be taken into account in case of experiments including monochromator. Resolution of monochromator is defined as the wavelength separation between two ideal monochromator spectral lines of equal intensity. Resolution is limited due to slit widths, optical aberrations and choice of gratings. Slit width choice is basic trade off. Wider monochromator entrance slits, allow more light to enter into the instrument. Narrower slits allow for better resolution between wavelengths, but enter less light from the source. Wavelength accuracy is the difference between the set wavelength and true wavelength [22]. Wavelength precision; is the gradation on the scale that the spectrometer uses in determining wavelength; of DK480 is 0.01 nm with 1200 g/mm grating and wavelength accuracy; the difference between the spectrometer's set wavelength and the true wavelength; is 0.3 nm with 1200 g/mm grating.

3.1.3 Integrating Sphere Technique

In this experimental setup, optical properties of biological tissues were calculated by using transmittance and reflectance measurements. There are three transmittance (Figure 3.9) and reflectance measurements (Figure 3.10). These are collimated transmittance (T_c), diffused transmittance (T_d), total transmittance (T_t), collimated reflectance (R_c), diffused reflectance (R_d) and total reflectance (R_t). After these measurements, these values were entered as an input to software which was developed for calculating optical properties.
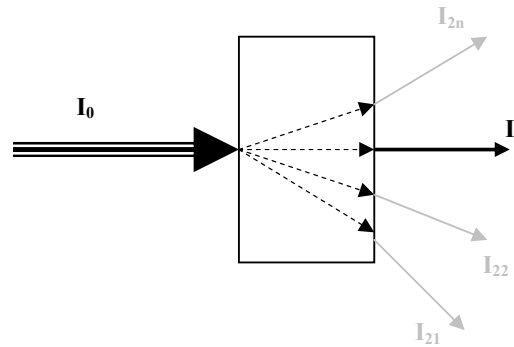
Figure 3.9 Transmittance of light in tissue.

Diffused Transmittance T_d is the ratio of incident light (I_0) and sum of light ($I_{21}+I_{22}+....I_{2n}$) which are transmitted to different directions from the incoming beam's pathway (Figure 3.9).

Collimated Transmittance T_c, is the ratio of the intensities of the incident light (I_0) and the light (I_1), which is, transmitted in the same direction that the incident beam's pathway (Figure 3.9).

Total Transmittance T_t is the ratio of the intensities of the incident light (I_0) and the total transmitted light (it contains both collimated and diffused transmitted light).

$$T_c + T_d = T_t \qquad (3.2)$$
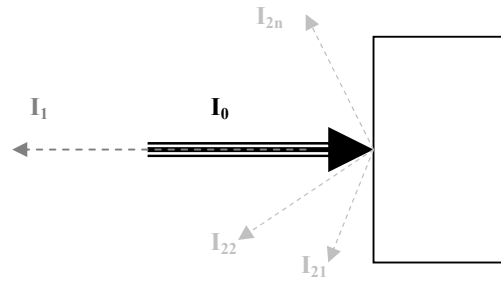
Figure 3.10 Reflectance of light in case of tissue-light interaction.

Diffused Reflectance R_d is the ratio of the intensities of the incident light (I_0) and the sum of light ($I_{21}+I_{22}+....I_{2n}$), which are reflected to different directions from the incoming beam's pathway (Figure 3.10).

Collimated Reflectance R_c is the ratio of the intensities of the incident light (I_0) and the light (I_1) which is reflected in the same direction that the incident beam's pathway (Figure 3.10).

Total Reflectance R_t is the ratio of the intensities of the incident light and the total reflected light (it contains both collimated and diffused reflected light).

$$R_d + R_c = R_t \tag{3.3}$$

Sum of total reflectance R_t, total transmittance T_t and total absorption must equal to "1".

$$R_t + T_t < 1 \tag{3.4}$$

Integrated sphere (Labsphere, IS-040-SL, North Sutton, USA) is used to measure the total transmittance, diffuse reflectance and the collimated transmittance values for any system which is used to evaluate optical properties of tissue [7]. To measure these values, ports of sphere are used. Often tissue is placed between glass plates to prevent dehydration and also to provide mechanical support. However the sphere theory requires that no

directly reflected light from the sample irradiates the detector; therefore baffle is placed between sample and detector [23].

All these transmittance and reflectance measurements are made by using different techniques.
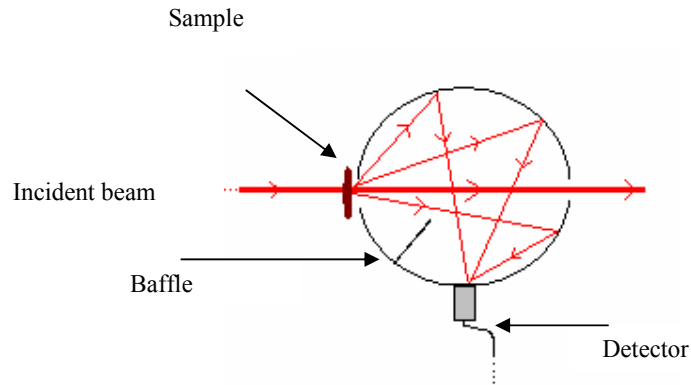
Figure 3.11 Diffused transmittance measurements by using integrating sphere.

Diffused transmittance T_d is measured by placing the sample to the front port of the sphere (Figure 3.11). By opening the back port of the sphere, so that the collimated transmittance goes out of the sphere through the back port
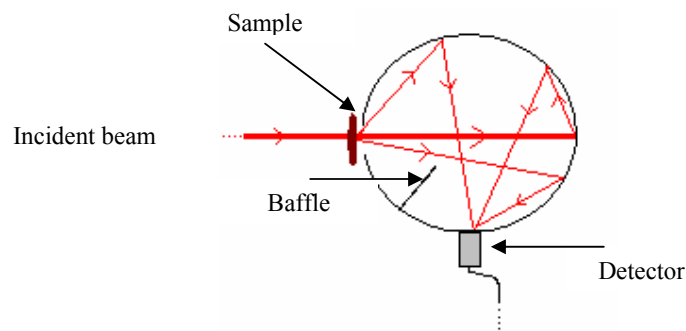
Figure 3.12 Total transmittance measurement by using integrating sphere.

In order to measure total transmittance T_t, the sample is located to the front port of the sphere and the back port of the sphere is closed (Figure 3.12).

Diffused reflectance R_d is measured by locating the sample to the back port of the sphere (Figure 3.13). Collimated reflectance goes out of the sphere through the front port .

Total reflectance R_t is measured by locating the sample to the back port of the sphere with a small inclination so that the collimated reflectance can not go out of the sphere (Figure 3.13).
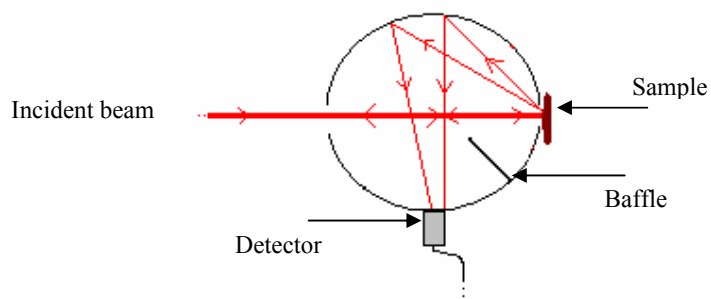
Figure 3.13 Diffused reflectance measurements by using integrating sphere.
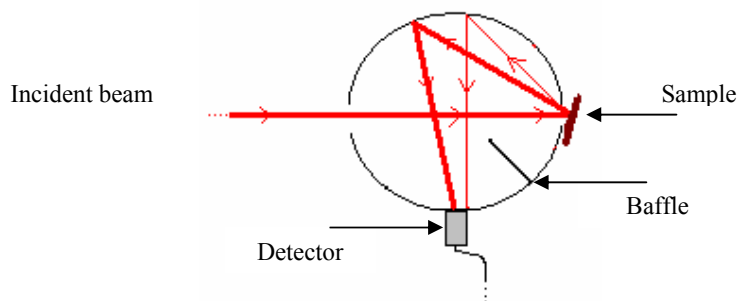
Figure 3.14 Total reflectance measurement by using integrating sphere.

Light that is emitted from the exit slit of monochromator is focused on integrating sphere by means of optical lenses individually. Systems for transmittance measurements and reflectance measurements are different. Before light reaches integrating sphere, it is chopped by a chopper (Figure 3.15). Light is focused on external grid of chopper SR540 (Figure 3.16), and it is controlled by a chopper controller which controls the chopper frequency. In order to carefully avoid noise frequencies such as line frequency and its entire odd and even harmonics, chopper frequency should be adjusted at specific values. Chopper controller was also connected to lock-in amplifier to lock frequency of reference input to the chopper frequency. Thus frequency always adjusted to 217Hz. Both accuracy and resolution of SR540 is 1 Hz [24].

Internal ring
Aperture : 124''

External ring
Aperture : 170''

Chopper diameter : 4 ''
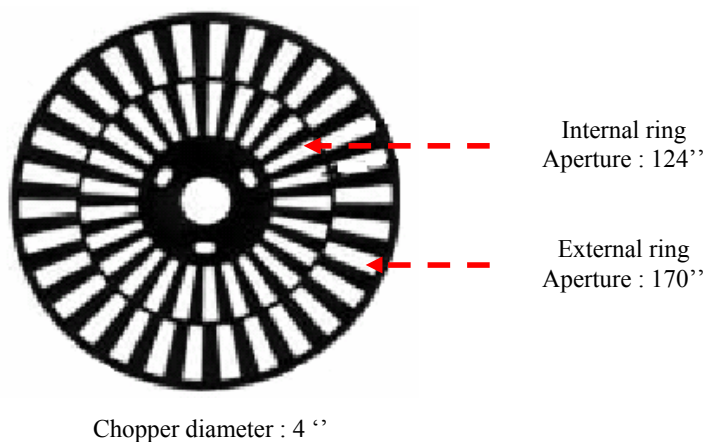
Figure 3.15 Chopper specifications [24].

After light passes through chopper, it is again focused on integrating sphere to get transmittance and reflectance measurements individually. Integrating sphere ports are used as mentioned above for all measurement values (T_t, T_d, R_t, R_d). Reflected and the transmitted light will be detected by a detector with a SR510 lock-in amplifier (Figure 3.17).
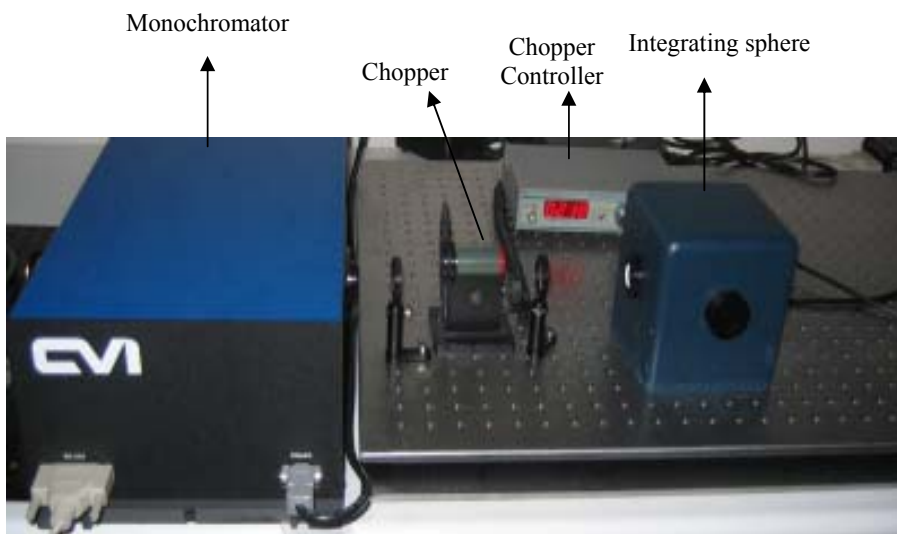
Figure 3.16 Optic lenses between monochromator and integrating sphere. Incoming light from exit slit of monochromator is focused on chopper firstly by means of first in order to chop light. Then light is focused onto integrating sphere by means of second lens.
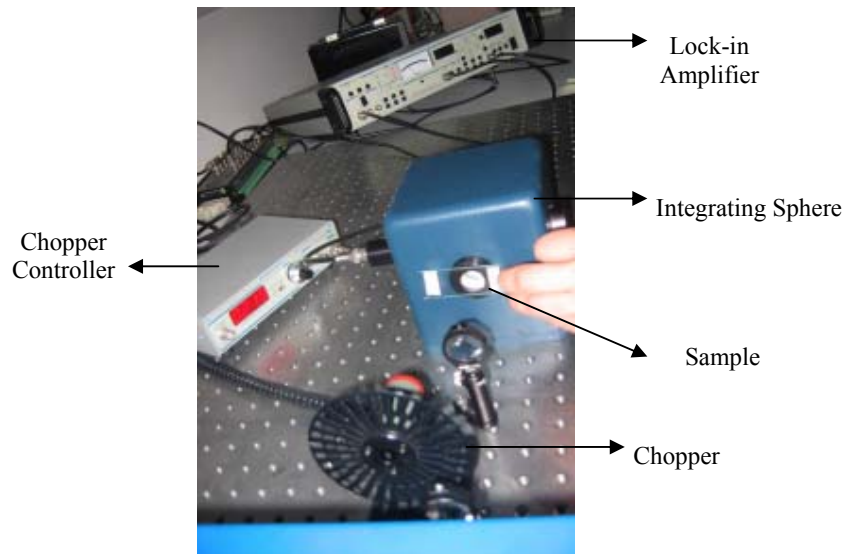
Figure 3.17 Integrating sphere technique. Measured data are detected by detector which is connected to lock-in amplifier. Amplified measured data are got from lock-in amplifier.

Lock-in technique is used to detect and measure very small ac signals. A Lock-in amplifier (Stanford Research Systems, SR510) can make accurate measurements of small signals even when the signals are obscured by noise sources which may be a thousand times larger [25]. A typical lock-in application may require a centre frequency of 10 KHz and a bandwidth of 0.01 Hz. Two signals are provided to the lock-in. The 1VAC reference is used to tell the lock-in the exact frequency of the signal of interest. The signal from the sample under test is amplified by a high gain ac coupled differential amplifier. The output of this amplifier is multiplied by the PLL output in the Phase-Sensitive Detector (PSD). This multiplication shifts each frequency component of the input signal. New signal has two components: sum component and a difference component. Sum frequency component is attenuated by the low pass filter, and only those difference frequency components within the low pass filter's narrow bandwidth will pass through to the dc amplifier. Since the low pass filter can have time constants up to 100 seconds, the lock-in can reject noise which is more than 0.025 Hz away from the reference frequency input [25].

Thus, to make signals in phase with reference signal, phase control should be usually adjusted for zero phase difference between the signal and the reference. This can be done by maximizing the output signal. Changing reference oscillator signal phase at

90° with respect to signal, phase control can be shifted by 90° to maximize the signal. Alternatively, since the phase control is well calibrated, the phase of the signal can be measured by adding 90° to the phase setting which nulls the signal. Aim of this calibration is to get zero phase shift between reference input and sample signal [25].

3.2   Preparation of Biological Tissues

3.2.1   Preparation of Native Biological Tissues

As mentioned before, aim of this study is to estimate optical properties of native and coagulated different *in vitro* lamb brain tissues. These tissues are cerebellar tissue, brainstem, frontal lobe cortical and sub cortical regions (Figure 3.18).
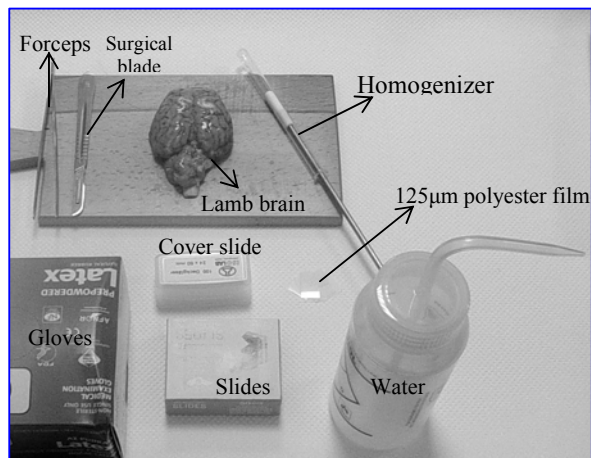
Figure 3.18 Tissue Preparation Tools.

3.2.2   Preparation of Coagulated Brain Tissues

Coagulation process is made 1.5 hours at three different temperatures (45°C±2, 60°C±2, and 80°C±2) for each tissue laboratory of Molecular Biology and Genetics

department of Bogazici University by using heat block. Heat block is a device which is used to make temperature stable during the coagulation process. After coagulation, measurements of these coagulated tissues are completed individually. Preparation and measurement of optical properties of these tissues are made after native tissue experiments were completed.

3.2.3   Homogenization and Slide Preparation of Tissues

Before any optical measurements, brain tissues are cut into smaller particles by using surgical blades. After this process, their sizes were available for homogenization (Figure 3.19). These small particles were put into a glass tube and squeezed by a metal stick. During this squash, some part of tissues were become liquid form and collected upper levels of tube. These liquid tissues were than used in sample preparation in order to get optical measurements. In sample preparation process (Figure 3.20), homogenized tissues were poured on the middle of glass slides and then they were covered with a cover slip. Between cover slip and glass slide, polyester film with 125μm thickness. This enables to give a quite accurate thickness to the tissue drop which is located in between the polyester films. These procedures are applied to both of coagulated and native tissues. For each wavelength measurements, 5 sample slides were prepared. In addition to this, in second step, plastic heating tubes were full of saline and native tissues were immersed into these tubes before they have been coagulated. Saline is used to remove hemoglobin, because hemoglobin is one of the chromophores which affect the optical properties of tissues.
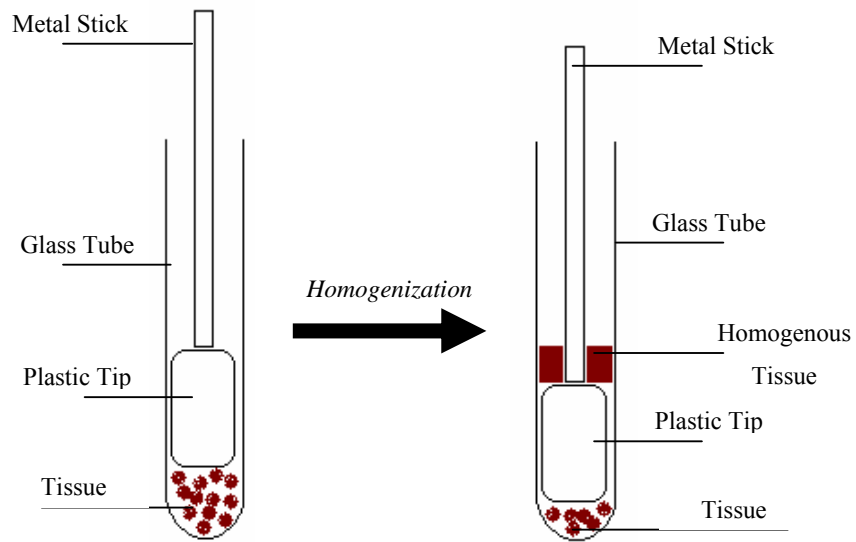
Figure 3.19 Homogenisation of Biological Tissue [26].
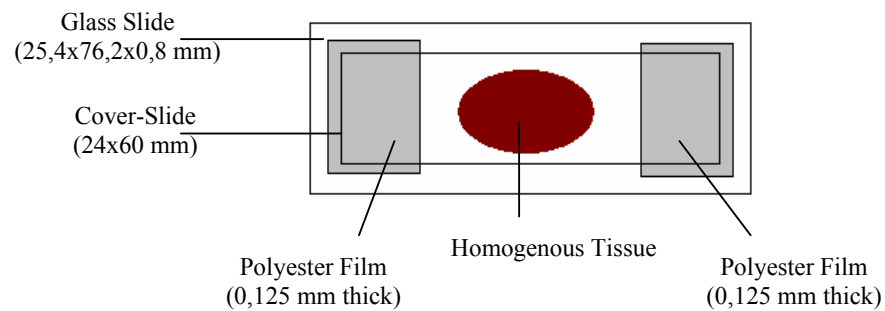
Figure 3.20 Sample slide preparation (Top view) [26].
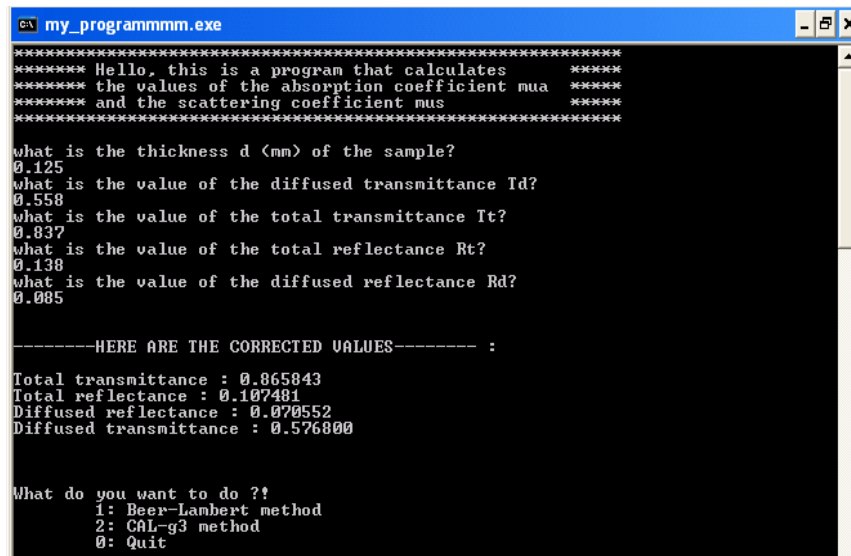
3.3. Estimation of Optical Properties of Biological Tissues

3.3.1. CAL-g3 Software

After measurements had been acquired from experimental setup by means of integrating sphere and lock-in amplifier, these values were evaluated in order to get optical

properties of each biological tissue. Estimation process was achieved by a software program called CAL-g3 which was developed in Biophotonics Laboratory.

CAL-g3 software program which estimates tissues' optical properties requires five inputs: Sample thickness, diffused transmittance, total transmittance, total reflectance and diffused reflectance (Figure 3.18). After these inputs were entered, optical properties (g, τ, μ_s, μ_a, μ_t, μ_s') of biological tissue would be determined. Since tissues were between two glass slides, due to glass-tissue interface, measured results should be corrected. CAL-g3 can also   makes these correction related to Kottler's formula.

Figure 3.21 CAL-g3 software interfaces. CAL-g3 software requires five inputs which are sample thickness, diffused transmittance, total transmittance, total reflectance and diffused reflectance.

4. RESULTS

After experimental optic system has been prepared, T_d, T_t, R_d and R_t measurements were begun. Firstly, in order to control precision of system, optical properties of native whole blood tissue were estimated for 6 different wavelengths and compared to the values reported in literature (Table 4.1, 4.2).

Table 4.1

Optical properties of native whole blood tissue.

λ (nm)	μ_a (mm^{-1})	μ_s (mm^{-1})	μ_s' (mm^{-1})	μ_t (mm^{-1})	α	τ (mm)	g
488	11,91± 0,14	48,13± 0,35	26,69± 0,23	60,43± 0,43	0,8± 0,01	0,016	0,44± 0,05
514	12,72± 0,17	41,75± 0,21	23,58± 0,2	54,48± 0,36	0,76± 0,03	0,018	0,43± 0.04
532	12,56± 0,06	36,34± 0,23	22,54± 0,15	48,9± 0,2	0,74	0,020	0,37± 0,01
633	1,38± 0,22	16,56± 0,34	6,07± 0,11	17,94± 0,3	0,92± 0.01	0,055	0,63± 0,01
810	1,92± 0,34	20,92± 0,45	4,60± 0.31	22,85± 0,26	0,91± 0.05	0,043	0,77
880	2,35 ±0,34	19,35± 0,62	4,02± 0,42	21,71± 0,38	0,89± 0.09	0,046	0,79± 0,02

Table 4.2

Comparision of results of this study and literature reports of whole blood tissue for 488-nm [27].

λ (nm)	μ_a (mm^{-1})	μ_s (mm^{-1})	τ (mm)
488-nm (study report)	11,91± 0,14	48,13± 0,35	0,016
488-nm (Literature report)	10,22	13.44	0.04

For 488-nm, our results were very close to literature results. There was a difference in scattering coefficient value. Scattering coefficient is related to experimental system. In literature, 488-nm Ar-ion laser was used whereas lamb was used as a light source in this study. Thus, scattering is always higher in experiments which use lamb as a light source than experimental systems use laser. But absorption coefficient value was very close to literature value. μ_a values of blood tissue are higher between 420-nm and 550-nm due to high absorption peaks of hemoglobin (Figure 2.3) [27]. At 633-nm, whole blood has one of the minimum μ_a values in visible range. like in this study.

Penetration depths of whole blood tissue for each wavelength were shown below (Figure 4.1):

Penetration Depth of Native Whole Blood Tissue
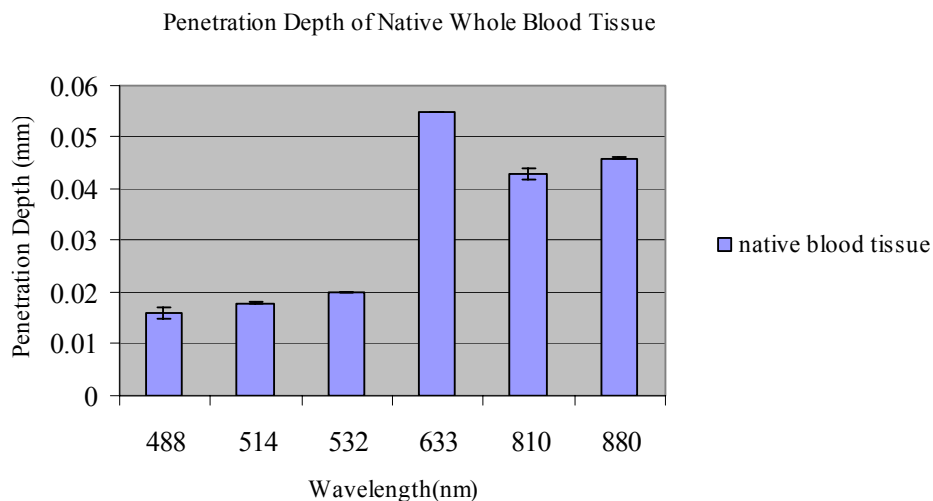
Figure 4.1 Penetration depths of whole blood tissue.

It was stated that, absorption coefficient of whole blood tissue dramatically decreases as the wavelength increases up to 633-nm. Thus, penetration depth of light inside blood tissue is maximum at 633-nm (Figure 4.1).

After determination of whole blood tissue characterization with this experimental setup, it was evident that our system was reliable. Then optical properties of different lamb brain tissues were estimated. After estimation of optical properties, tissue similarities for each wavelength were determined applying t-test for absorption and scattering

coefficients of native tissues (Table 4.3, 4.4). By means of t-test, not only tissue similarities were determined, but also significant differences of optical properties (μ_a, μ_s) of each native tissue due to wavelength change were determined (Table 4.5, 4.6).

Table 4.3

Absorption coefficients of native brain tissues. Significantly differences between grey matter (GM), white matter (WM), cerebellar tissue (C) and brainstem (B) tissues are shown.

λ (nm)	Frontal lobe grey Matter μ_a (mm^{-1})	Frontal lobe white matter μ_a (mm^{-1})	Brainstem μ_a (mm^{-1})	Cerebellar tissue μ_a (mm^{-1})	Significantly Different Tissues (p<0,05)
488	0,99±0,35	2,56±0,16	1,96±0,17	0,56±0,37	GM-B, GM-C, WM-C, B-C, GM-WM
514	1,53±0,44	2,52±0,16	1,83±0,19	0,72±0,17	B-C, GM-WM, B-GM, C-GM, C-WM
532	0,96±0,13	2,59±0,09	1,91±0,04	0,59±0,44	GM-WM, B-GM, C-GM, C-WM, B-C
633	0,72±0,41	2±0,13	1,23±0,25	0,34±0,24	All tissues except GM-C
780	1,24±0,13	2,23±0,21	1,57±0,34	0,74±0,3	All tissues except GM-C
810	1,1±0,08	2,83±0,41	0,92±0,4	0,65±0,23	WM-GM, WM-B, WM-C, GM-C
880	1,39±0,09	2,34±0,2	1,89±0,31	1,74±0,29	GM-WM, GM-B, GM-C
905	1,38±0,23	2,15±0,36	1,70±0,53	0,97±0,34	GM-WM, GM-C, WM-C

It was stated that absorption coefficients of cerebellar tissue, white matter and brainstem tissues were higher within hemoglobin absorption band (Table 4.3). Hemoglobin has one of the minimum absorption coefficient values at 633-nm (Table 4.1). Thus, minimum μ_a was stated at 633-nm for all brain tissues.

Table 4.4

Scattering coefficients of native brain tissues. Significantly differences between grey matter (GM), white matter (WM), cerebellar tissue (C) and brainstem (B) tissues are shown.

λ (nm)	Frontal lobe grey matter μ_s (mm^{-1})	Frontal lobe white matter μ_s (mm^{-1})	Brainstem μ_s (mm^{-1})	Cerebellar tissue μ_s (mm^{-1})	Significantly Different Tissues (p<0,005)
488	17,89±0,35	24,4±0,17	19,87±0,26	19,3±3,15	GM-WM, GM-C, WM-C, B-C
514	10,91±3,81	26,48±1,46	18,83±1,63	17,16±1,4	GM-WM,WM-C, WM-B, B-C
532	16,85±0,7	22,35±0,09	17,35±0,26	17,56±0,035	GM-WM, WM-B, WM-C
633	16,53±1,49	21,15±0,14	17,48±5	15,5±0,185	GM-WM, WM-B,
780	10,47±0,13	21,73±1,59	14,46±0,33	15,45±0,72	GM-WM, WM-B, WM-C
810	7,3±0,09	20,45±0,22	14,83±0,27	15,78±1,4	GM-WM, WM-B, WM-C
880	8,79±0,09	17,52±0,38	15,03±0,85	8,64±0,19	GM-C, WM-C, WM-B, C-B
905	7,36±1,31	19,76±1,18	15,43±0,94	14,32±0,04	GM-WM, WM-B, WM-C

It was stated that, scattering coefficients of all native tissues decreases as wavelength increases (Table 4.4). Because as wavelength increases, rayleigh scattering decreases and mie scattering increases [3].

Table 4.5

Significantly differences of μ_a values of native tissues related to wavelength.

Tissue	488-nm p<0,05	514-nm p<0,05	532-nm p<0,05	633-nm p<0,05	780-nm p<0,05	810-nm p<0,05	880-nm p<0,05	905-nm p<0,05
White Matter	633	633 780	780	780 880	514 633	–	633	–
Grey Matter	633	633 880	780 810 880 905	488 514 780 810 880 905	633 532	532 633 880	514 532 633 810	532 633
Cerebellar tissue	880 905	633 880 905	880 905	514 810 880 905	880	633 880 905	with all wave lengths	488 514 532 633 810 880
Brainstem	633 532 780 810	633 810	633 780 810	488 514 532 880 905	488 532 810	488 514 532 780 880 905	633 810	633 810

In table 4.5 and table 4.6, significant differences of optical properties (μ_a, μ_s) of each native tissue due to wavelength change were determined. It was stated that significant differences in absorption coefficients for each tissue increased as wavelength increased through near infrared region (Table 4.5). Saline solution was not used in native tissue experiments, thus hemoglobin was not removed from tissues. Hemoglobin absorption spectra affected significances in all tissues due to wavelength change [28].

It was observed that significant differences in scattering coefficients for each tissue increased as wavelength increased through near infrared region (Table 4.6). Especially this situation was very clear for white matter and brainstem.

Table 4.6

Significantly differences of μ_s values of native tissues related to wavelength.

Tissue	488-nm p<0,05	514-nm p<0,05	532-nm p<0,05	633-nm p<0,05	780-nm p<0,05	810-nm p<0,05	880-nm p<0,05	905-nm p<0,05
White Matter	633 780 810 880 905	633 780 810 880 905	633 780 810 880 905	780	488 514 532 633	488 514 532 880	488 514 532 810	488 514 532
Grey Matter	780 810	905	810 880 905	810 880	488	488 880 633	532 633 810	532
Cerebellar tissue	880	880	780	810 880 905	880	880	With all wavelengths	633 880
Brainstem	780 810 880 905	780 810 880 905	780	–	488 514 532	488 514	488 514	488 514

Optical properties of coagulated brain tissues at different temperatures were also estimated. After these properties had been calculated, anova test was applied. Both native and coagulated tissue values set as a group. While specific tissue and its coagulated values were group, only temperature was changed for each group. Aim of anova test is to investigate significant differences of scattering and absorption coefficients between coagulated and native tissues as temperature changes for same wavelength.

Related to anova test for brainstem tissue absorption coefficients, absorption coefficient values of groups were significantly different from each other for all wavelengths (Table 4.7). It was also stated as tissue was coagulated, absorption values increased. But this increase was not proportional to temperature rise (Figure 4.2).

Scattering coefficients of native and coagulated brainstem tissues were estimated and significant differences were determined by means of anova test (Table 4.8). Scattering coefficient values of native and coagulated tissues were significantly different from each other for all wavelengths ($F \gg F_{critical}$). Also it is evident that as tissue was coagulated, scattering coefficient values increased (Figure 4.3). It was said that μ_a and μ_s were higher in coagulated tissues than native tissues.

Table 4.7

Absorption coefficients (mm^{-1}) of native and coagulated brainstem tissue.

λ (nm)	Brainstem (native)	Brainstem (45°C)	Brainstem (60°C)	Brainstem (80°C)	Significant differences (F>>F$_{critical}$)
488	1,96±0,175	2,36±0,3	3,29±0,26	3,37±0,35	F>>F$_{critical}$
514	1,83±0,19	2,37±0,11	3,1±0,25	3,17±0,36	F>>F$_{critical}$
532	1,91±0,049	2,38±0,3	3,01±0,19	2,99±0,33	F>>F$_{critical}$
633	1,23±0,175	1,78±0,25	2,64±0,25	2,16±0,29	F>>F$_{critical}$
780	1,57±0,19	2,06±0,34	3,23±0,25	2,59±0,36	F>>F$_{critical}$
810	0,92±0,049	1,83±0,44	3,04±0,27	2,41±0,11	F>>F$_{critical}$
880	1,89±0,31	1,95±0,39	3,26±0,25	2,54±0,35	F>>F$_{critical}$
905	1,70±0,53	1,92±0,19	2,99±0,25	2,38±0,46	F>>F$_{critical}$

Figure 4.2 Absorption coefficients of native and coagulated brainstem tissue.

Table 4.8

Scattering coefficients (mm^{-1}) of native and coagulated brainstem tissue.

λ (nm)	Brainstem (native)	Brainstem (45°C)	Brainstem (60°C)	Brainstem (80°C)	Significant differences (F>>F$_{critical}$)
488	19,87±0,26	25,69±0,31	29,49±1,35	23,87±0,46	F>>F$_{critical}$
514	18,83±1,62	25,1±0,13	28,2±0,71	23,3±0,06	F>>F$_{critical}$
532	17,35±0,26	24,55±0,31	26,35±1,81	23,48±0,26	F>>F$_{critical}$
633	17,48±5,01	23,52±0,26	27,07±0,33	21,32±0,35	F>>F$_{critical}$
780	14,46±0,33	21,67±0,92	23,95±1,53	20,21±0,14	F>>F$_{critical}$
810	14,83±0,27	22,27±0,38	23,39±0,94	19,37±1,09	F>>F$_{critical}$
880	15,03±0,85	20,64±0,39	21,61±0,56	19,23±0,32	F>>F$_{critical}$
905	15,43±0,94	20,67±0,19	23,66±0,14	18,86±0,52	F>>F$_{critical}$

Absorption coefficients of native and coagulated cerebellar tissue tissues were estimated and significant differences were determined by means of anova test (Table 4.9). For cerebellar tissue as temperature increased, absorption coefficients were also increased (Figure 4.4). As a result of anova tests, absorption coefficients of native and coagulated cerebellar tissue brain tissues were significantly different from each other(F>>F$_{critical}$)

Scattering coefficients of native and coagulated cerebellar tissue tissues were estimated and significant differences were determined by means of anova test (Table 4.10). It was observed that maximum scattering coefficient values were calculated at 60°C. For 45°C and 80°C, in 488-nm, 633-nm, 810-nm and 880-nm, scattering coefficient values were highest at 45°C (Figure 4.5).
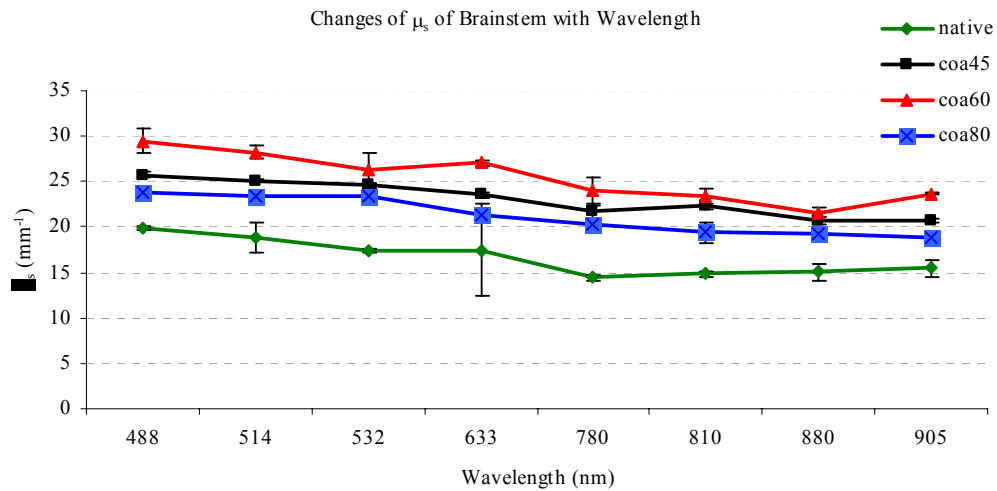
Figure 4.3 Scattering coefficients of native and coagulated brainstem tissue.

Table 4.9

Absorption coefficients (mm^{-1}) of native and coagulated cerebellar tissue.

λ (nm)	Cerebellar tissue (Native)	Cerebellar tissue (45°C)	Cerebellar tissue (60°C)	Cerebellar tissue (80°C)	Significant differences (F>>F$_{critical}$)
488	0,56 ±0,37	0,69 ±0,33	2,05 ±0,3	2,48 ±0,15	F>>F$_{critical}$
514	0,72 ±0,17	0,67 ±0,24	1,94 ±0,79	2,38 ±0,22	F>>F$_{critical}$
532	0,592±0,44	0,64 ±0,1	1,81 ±0,11	2,26 ±0,12	F>>F$_{critical}$
633	0,340±0,24	0,54 ±0,4	1,34 ±0,85	1,45 ±0,11	F>>F$_{critical}$
780	0,741 ±0,3	0,99 ±0,17	1,6 ±1,06	1,51 ±0,5	F>>F$_{critical}$
810	0,65 ±0,23	0,94 ±0,1	1,49 ±0,11	2,75 ±0,45	F>>F$_{critical}$
880	1,744±0,29	1,14 ±0,07	1,62 ±0,3	1,56 ±0,14	F>>F$_{critical}$
905	0,975±0,34	0,99 ±0,09	1,49 ±0,21	1,48 ±0,09	F>>F$_{critical}$

Absorption and scattering coefficients of native and coagulated grey matter tissues were estimated and it was stated that both μ_a and μ_s values were significantly different from each other due to anova test results for all wavelengths (Table 4.11, 4.12). μ_a values

of coagulated tissues were higher than native grey matter tissue (Figure 4.6). While maximum absorption coefficient values were acquired at 80°C at 488-nm, 514-nm, 532-nm, at 633-nm, 780-nm, 810-nm, 880-nm and 905-nm maximum μ_a values were got at 45°C.
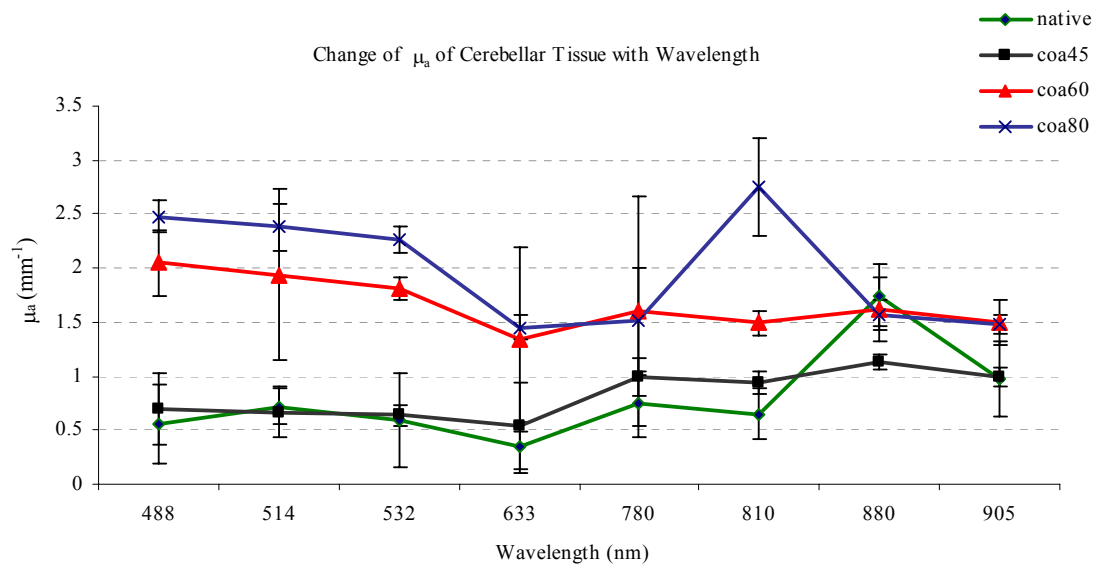
Figure 4.4 Absorption coefficients of native and coagulated cerebellar tissue.

It is evident that, scattering coefficients of coagulated frontal lobe grey matter tissues were higher than native tissues at all wavelengths (Table 4.12). Scattering coefficients values at 60°C at 488-nm, 514-nm and 532-nm were highest (Figure 4.7). As wavelength increased through near infrared, scattering coefficients increased due to increase in mie scattering and decrease in rayleigh scattering. At 633-nm, 780-nm, 810-nm, 880-nm and 905-nm μ_s values were biggest at 80°C.

Table 4.10

Scattering coefficients (mm^{-1}) of native and coagulated cerebellar tissue.

λ (nm)	Cerebellar tissue (native)	Cerebellar tissue (45°C)	Cerebellar tissue (60°C)	Cerebellar tissue (80°C)	Significant differences (F>>F$_{critical}$)
488	19,3±3,15	19,9±0,3	24,35±0,19	20,6±0,22	F>>F$_{critical}$
514	17,16±1,4	18,79±0,79	24,22±1,22	19,79±0,22	F>>F$_{critical}$
532	17,56±0,035	18,82±0,11	22,66±0,31	19,91±0,12	F>>F$_{critical}$
633	15,5±0,18	18,81±1,85	20,82±0,04	17,47±0,12	F>>F$_{critical}$
780	15,45±0,72	16,55±1,06	19,46±0,44	16,76±0,41	F>>F$_{critical}$
810	15,78±1,4	17,02±0,11	19,82±0,6	10,16±0,48	F>>F$_{critical}$
880	8,64±0,19	16,48±0,21	19,81±0,3	14,94±0,57	F>>F$_{critical}$
905	14,32±0,04	16,15±0,21	18,51±1,14	14,88±0,09	F>>F$_{critical}$

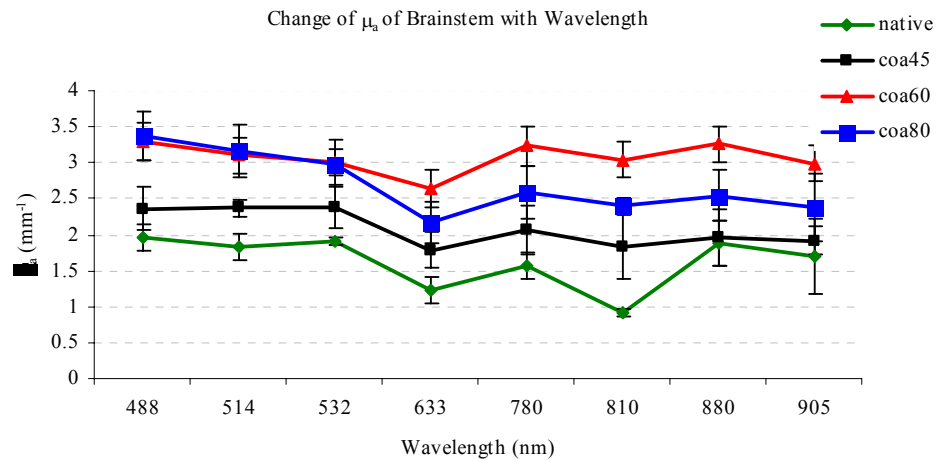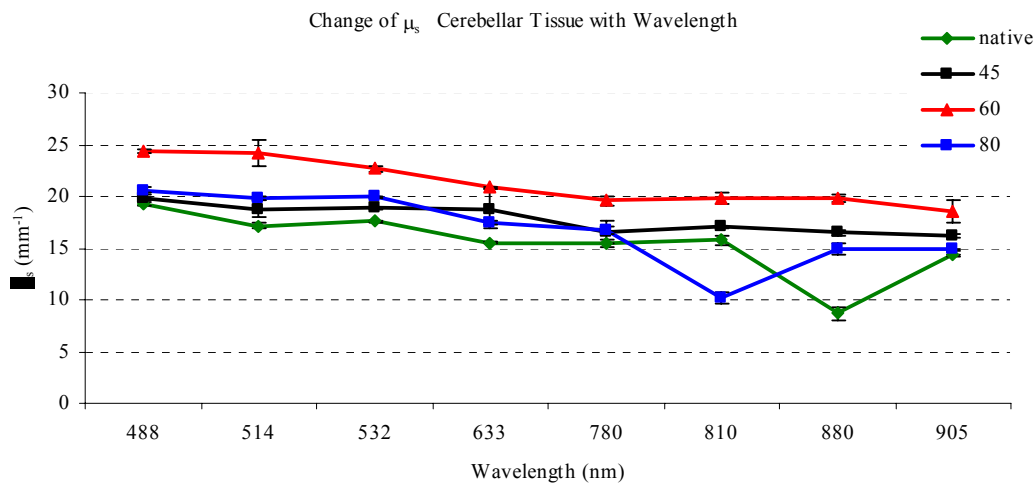**Figure 4.5** Scattering coefficients of native and coagulated cerebellar tissue.

Figure 4.6 Absorption coefficients of native and coagulated grey matter tissue.

Table 4.11

Absorption coefficients of native and coagulated frontal lobe grey matter tissue.

λ (nm)	Grey Matter (Native)	Grey Matter (45°C)	Grey Matter (60°C)	Grey Matter (80°C)	Significant differences (F>>$F_{critical}$)
488	0,99±0,35	1,17±0,22	2,07±0,32	2,09±0,23	F>>$F_{critical}$
514	1,53±0,44	1,35±0,11	1,94±0,39	1,97±0,18	F>>$F_{critical}$
532	0,96±0,13	1,36±0,08	1,77±0,22	1,85±0,19	F>>$F_{critical}$
633	0,72±0,41	1,46±0,17	1,21±0,22	1,25±0,14	F>>$F_{critical}$
780	1,24±0,13	2,74±0,37	1,56±0,11	1,56±0,13	F>>$F_{critical}$
810	1,1±0,08	2,75±0,29	1,51±0,18	1,54±0,12	F>>$F_{critical}$
880	1,39±0,09	3,23±0,43	1,63±0,13	1,61±0,13	F>>$F_{critical}$
905	1,38±0,23	3,5±0,36	1,59±0,12	1,59±0,11	F>>$F_{critical}$

Table 4.12

Scattering coefficients of native and coagulated frontal lobe grey matter tissue.

λ (nm)	Grey Matter (Native)	Grey Matter (45°C)	Grey Matter (60°C)	Grey Matter (80°C)	Significant differences (F>>F_{critical})
488	17,89±0,35	21,22±3,12	22,6±1,2	22,57±0,33	F>>F_{critical}
514	10,91±3,81	20,21±3,97	21,97±0,5	21,94±0,37	F>>F_{critical}
532	16,85±0,7	18,67±2,58	22,51±0,14	22,05±0,09	F>>F_{critical}
633	16,53±1,4	15,83±0,58	20,52±0,18	21,04±1	F>>F_{critical}
780	10,47±0,13	14,12±0,98	19,24±0,25	20,41±0,93	F>>F_{critical}
810	7,3±0,09	14,51±2,5	18,6±0,15	19,03±0,29	F>>F_{critical}
880	8,79±0,09	14,81±1,4	18,36±0,04	17,95±0,33	F>>F_{critical}
905	7,36±1,31	12,84±1	18,62±0,05	17,77±0,049	F>>F_{critical}
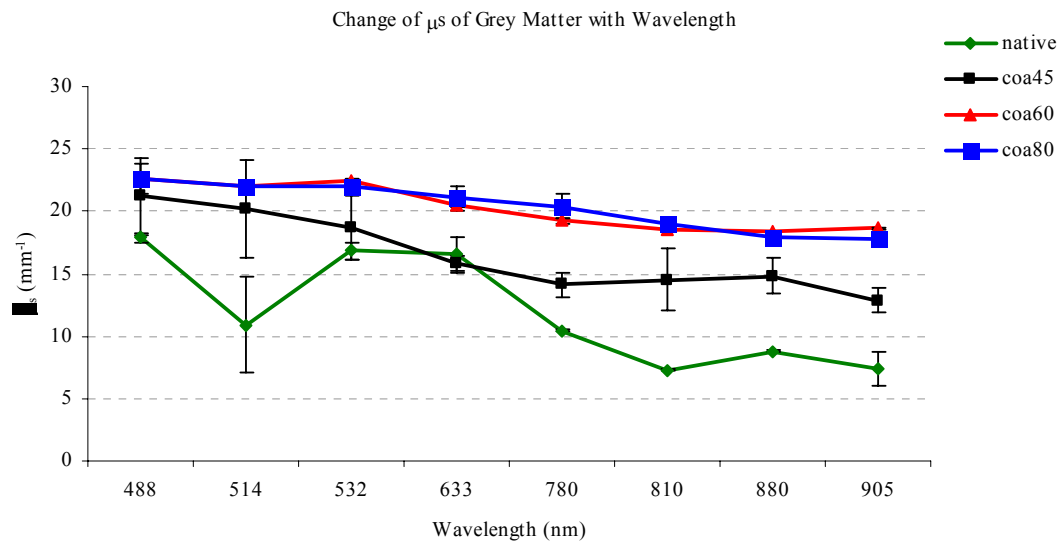
Figure 4.7 Scattering coefficients of native and coagulated grey matter tissue.

Absorption and scattering coefficients of native and coagulated white matter tissues were estimated and it was stated that both μ_a and μ_s values were significantly different

from each other due to anova test results for all wavelengths (Table 4.13, 4.14). It was stated that at 488-nm, 514-nm and 633-nm, maximum absorption coefficients were observed at 80°C. However at 532-nm, 780-nm, 880-nm and 905-nm absorption coefficients were highest at 60°C (Figure 4.8). Scattering coefficients of coagulated frontal lobe white matter tissues were higher than native tissue coefficients (Table 4.14). Whereas maximum scattering was observed at 488-nm, 514-nm, 532-nm, 780-nm, 810-nm, 880-nm and 905-nm at 60°C, at 633-nm maximum scattering was estimated at 80°C (Figure 4.9). at 514-nm, scattering coefficient of native white matter was higher than value coagulated at 45°C.

Table 4.13

Absorption coefficients of native and coagulated frontal lobe white matter tissue.

λ (nm)	White matter (native)	White matter (45°C)	White matter (60°C)	White matter (80°C)	Significant differences (F>>F$_{critical}$)
488	2,56±0,16	2,4±0,58	2,76±0,26	2,93±0,15	F>>F$_{critical}$
514	2,52±0,16	1,89±0,96	2,68±0,25	2,77±0,19	F>>F$_{critical}$
532	2,59±0,09	2,59±0,57	2,73±0,16	2,72±0,22	F>>F$_{critical}$
633	2±0,13	1,27±0,52	2,09±0,18	2,16±0,15	F>>F$_{critical}$
780	2,23±0,21	2,66±0,56	2,72±0,36	2,6±0,23	F>>F$_{critical}$
810	2,83±0,41	2,59±0,45	2,7±0,4	2,55±0,23	F>>F$_{critical}$
880	2,34±0,36	2,9±0,56	2,94±0,26	2,63±0,21	F>>F$_{critical}$
905	2,15±0,2	2,77±0,49	2,92±0,24	2,54±0,24	F>>F$_{critical}$

Penetration depth of light inside tissue is related to light-tissue interaction. As energy dissipation due to scattering and absorption inside biological tissue increases, penetration depth of light decreases [4]. For brainstem it was observed that maximum penetration depths were estimated for native values (Table 4.15, Figure 4.10). Concerning cerebellar tissue tissue, maximum depths were calculated for native tissue samples except 488-nm (Table 4.16, Figure 4.11).

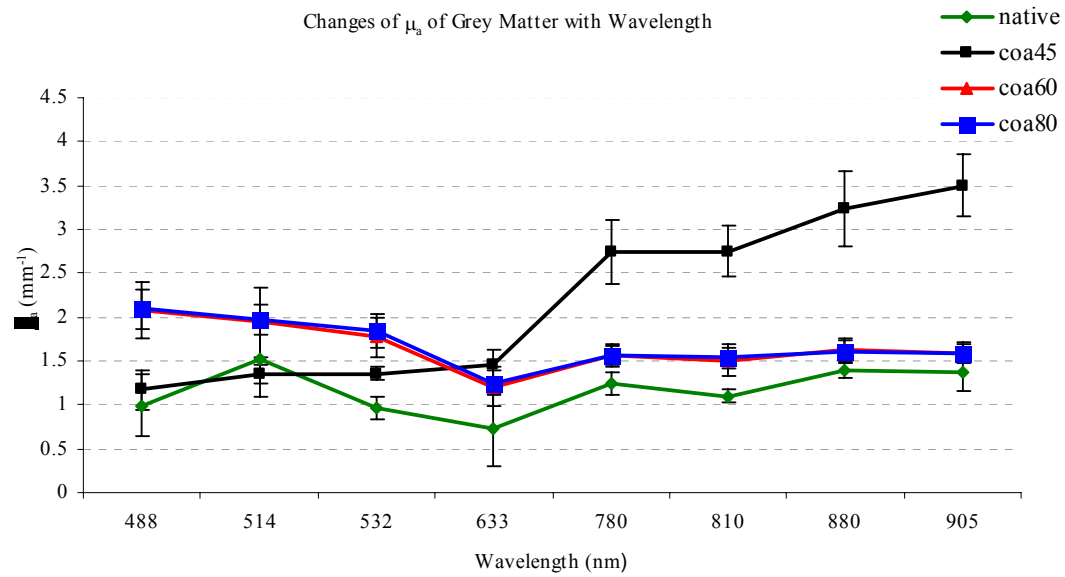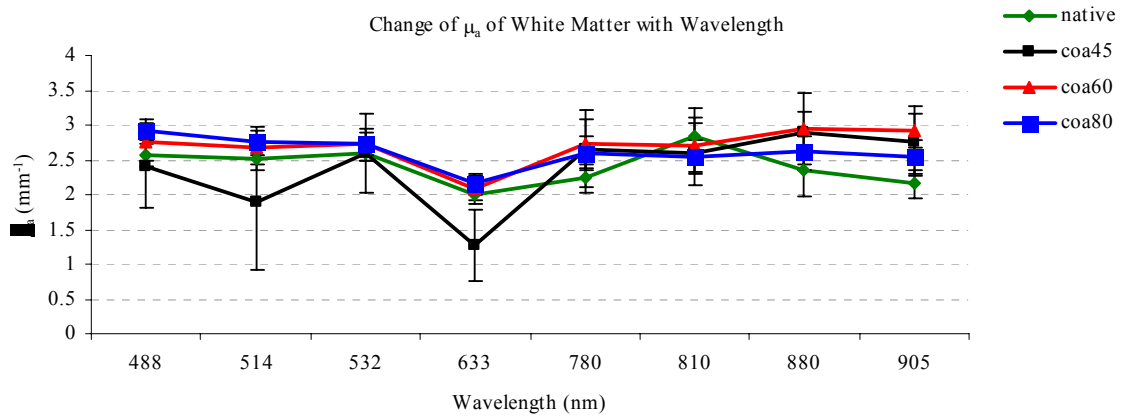**Figure 4.8** Absorption coefficients of native and coagulated white matter tissue.
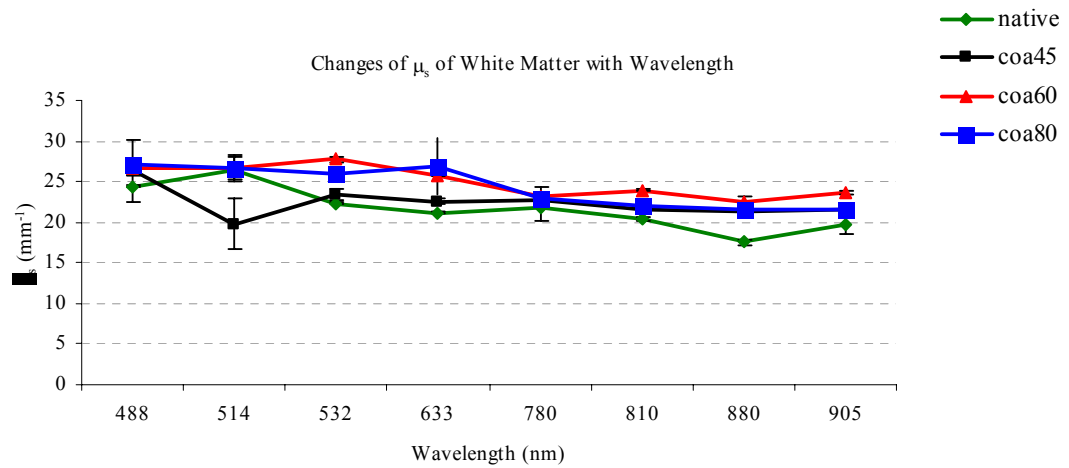
Figure 4.9 Scattering coefficients of native and coagulated white matter tissue.

Table 4.14

Scattering coefficients of native and coagulated frontal lobe white matter tissue.

λ (nm)	White matter (native)	White matter (45°C)	White matter (60°C)	White matter (80°C)	Significant differences ($F \gg F_{critical}$)
488	24,4±0,17	26,35±3,84	26,63±0,99	27,16±0,6	$F \gg F_{critical}$
514	26,48±1,46	19,79±3,13	26,7±1,51	26,59±0,1	$F \gg F_{critical}$
532	22,35±0,09	23,40±0,69	27,7±0,42	25,97±0,27	$F \gg F_{critical}$
633	21,15±0,14	22,55±0,35	25,73±0,1	26,84±3,41	$F \gg F_{critical}$
780	21,73±1,59	22,69±0,3	23,26±1,02	22,9±0,02	$F \gg F_{critical}$
810	20,45±0,22	21,56±0,1	23,99±0,09	21,94±0,71	$F \gg F_{critical}$
880	17,52±0,38	21,36±0,3	22,57±0,72	21,47±0,61	$F \gg F_{critical}$
905	19,76±1,18	21,61±0,2	23,75±0,24	21,55±0,16	$F \gg F_{critical}$

Table 4.15

Penetration depths of native and coagulated brainstem tissue.

λ (nm)	Brainstem (native)	Brainstem (45°C)	Brainstem (60°C)	Brainstem (80°C)
488	0,045	0,035	0,03	0,036
514	0,048	0,036	0,031	0,037
532	0,051	0,037	0,034	0,037
633	0,053	0,039	0,033	0,042
780	0,062	0,042	0,036	0,043
810	0,063	0,041	0,037	0,045
880	0,059	0,044	0,04	0,045
905	0,058	0,044	0,037	0,047
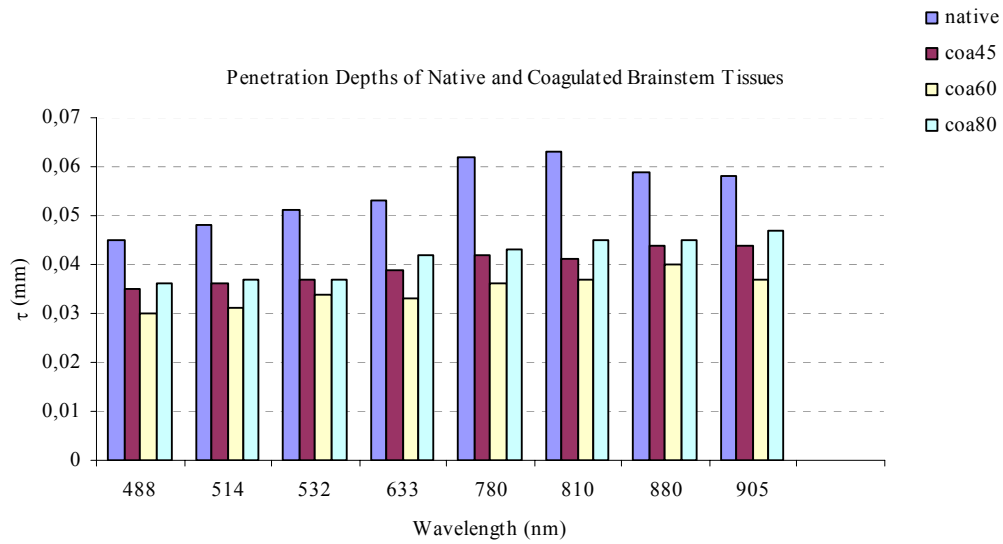
Figure 4.10 Penetration depths of native and coagulated brainstem tissue.
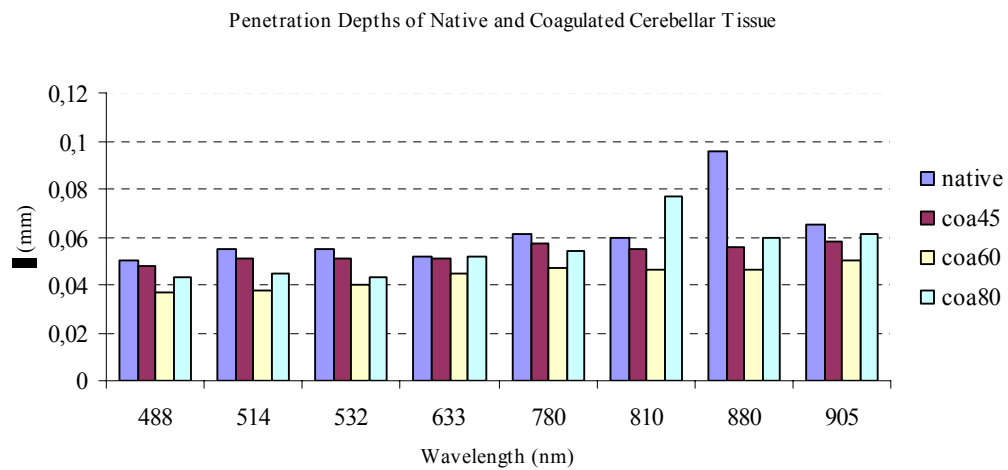
Figure 4.11 Penetration depths of native and coagulated cerebellar tissue.

Penetration depths of light through frontal lobe cortical (Table 4.17) and subcortical regions (Table 4.18), it was stated that light penetrates deeper in native tissues. Maximum penetration depth for grey mater tissue was observed at 810-nm for native tissue

(Figure 4.12). However, maximum penetration depth was observed at 905-nm for white matter native tissue (Figure 4.13). But at 514-nm, observed penetration depth at 45°C was higher than native value for white matter tissue.

Table 4.16

Penetration depths of native and coagulated cerebellar tissue.

λ (nm)	Cerebellar tissue (native)	Cerebellar tissue (45°C)	Cerebellar tissue (60°C)	Cerebellar tissue (80°C)
488	0,05	0,048	0,037	0,043
514	0,055	0,051	0,038	0,045
532	0,055	0,051	0,04	0,043
633	0,052	0,051	0,045	0,052
780	0,061	0,057	0,047	0,054
810	0,06	0,055	0,046	0,077
880	0,096	0,056	0,046	0,06
905	0,065	0,058	0,05	0,061

Table 4.17

Penetration depths of native and coagulated frontal lobe grey matter tissue.

λ (nm)	Grey Matter (native)	Grey Matter (45°C)	Grey Matter (60°C)	Grey Matter (80°C)
488	0,052	0,044	0,04	0,04
514	0,08±0,01	0,046	0,041	0,041
532	0,056	0,049	0,041	0,041
633	0,057	0,057	0,045	0,044
780	0,085	0,075	0,048	0,045
810	0,11	0,099	0,049	0,048
880	0,098	0,083±0,01	0,05	0,051
905	0,1	0,092	0,049	0,051

Table 4.18

Penetration depths of native and coagulated frontal lobe white matter tissue.

λ (nm)	White matter (native)	White matter (45°C)	White matter (60°C)	White matter (80°C)
488	0,037	0,034	0,034	0,033
514	0,034	0,046	0,034	0,034
532	0,04	0,038	0,032	0,034
633	0,043	0,041	0,035	0,034
780	0,041	0,039	0,038	0,039
810	0,042	0,041	0,037	0,040
880	0,05	0,041	0,039	0,041
905	0,045	0,037	0,037	0,041
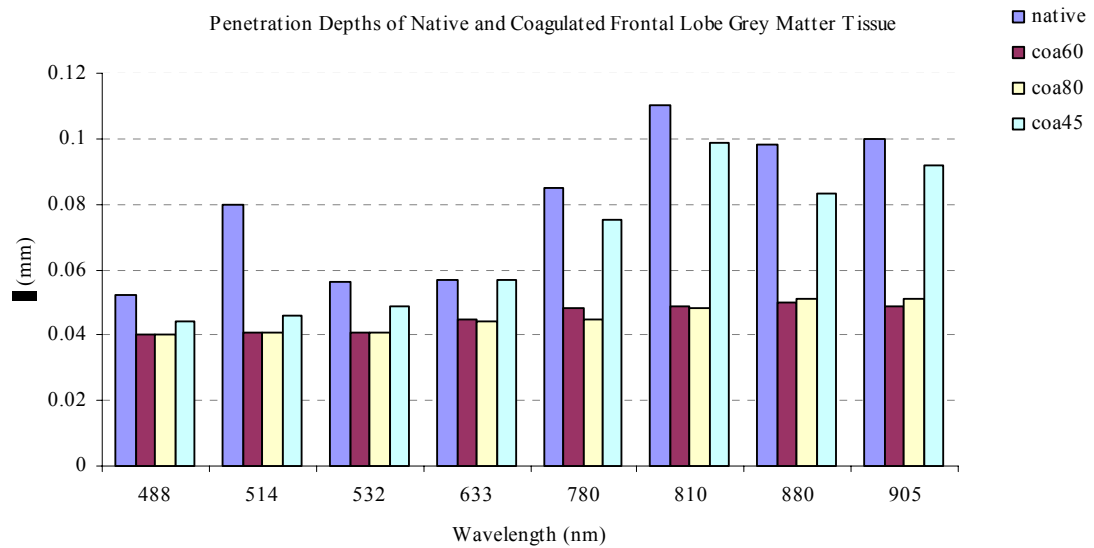
Figure 4.12 Penetration depths of native and coagulated grey matter tissue.

Penetration Depths of Native and Coagulated Frontal Lobe White matter Tissue

- native
- coa60
- coa80
- coa45
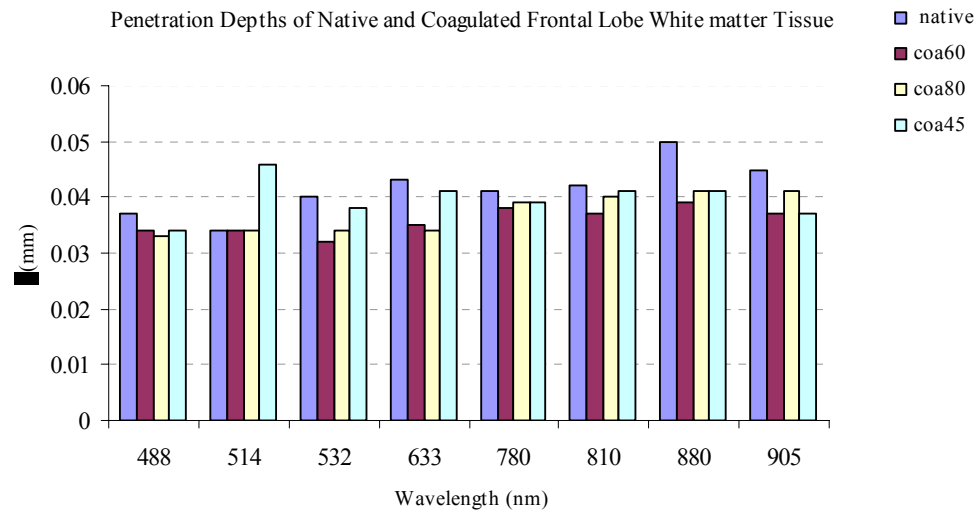
Figure 4.13 Penetration depths of native and coagulated white matter tissue.

Table 4.19

Total attenuation coefficients of native and coagulated brainstem tissue.

λ (nm)	Brainstem (native)	Brainstem (45°C)	Brainstem (60°C)	Brainstem (80°C)
488	21,84±0,45	28,05±0,41	32,7±1,54	28,04±0,87
514	20,67±1,98	27,48±0,74	31,3±0,91	27,29±0,95
532	19,26±0,31	26,93±0,54	29,37±2,29	27,29±0,59
633	18,72±7,61	25,3±0,78	29,72±0,91	24,13±0,78
780	16,03±0,65	23,74±1,11	27,19±1,96	23,63±0,85
810	15,76±0,75	24,1±0,96	26,43±1,25	22,59±1,95
880	16,92±0,94	22,59±0,82	24,87±1,05	22,64±0,74
905	17,14±1,28	22,59±0,62	26,66±0,88	22,11±1,05

Table 4.20

Albedo of native and coagulated brainstem tissue.

λ (nm)	Brainstem (native)	Brainstem (45°C)	Brainstem (60°C)	Brainstem (80°C)
488	0,909±0.03	0,915±0,01	0,899±0.03	0,876±0.04
514	0,911±0,02	0,913±0.03	0,9±0,01	0,88±0.04
532	0,9±0,02	0,911±0.03	0,897±0,02	0,886±0.03
633	0,934±0,02	0,929±0.05	0,91±0.03	0,907±0.03
780	0,901±0,02	0,912±0.03	0,881±0,01	0,886±0.03
810	0,941±0.03	0,924±0.03	0,884±0,02	0,889±0,02
880	0,887±0,01	0,913±0.04	0,868±0,01	0,883±0,02
905	0,9±0.05	0,914±0,01	0,887±0,02	0,887±0,01

Other important optical properties of any tissue are total attenuation coefficient, albedo, anisotropy factor and reduced scattering coefficients which were also be estimated in this project for each tissue. Total attenuation coefficient (μ_t) affects penetration depths of light into the tissue. For brainstem, maximum μ_t were acquired at 60°C (Table 4.19). Thus, minimum penetration of light for this tissue was observed at this temperature value. Albedo values of brainstem tissue were between 0 and 1, but closer to 1 for all wavelengths and temperatures (Table 4.20). This means that biological brainstem tissues were turbid media and scattering of light was considerably higher than absorption for both native and coagulated brain tissues. Anisotropy factor and reduced coefficients were estimated for brainstem tissue (Table 4.21, 4.22). As mentioned in chapter 2, anisotropy factor is the mean cosine of scattering angle. Anisotropy factors of all brainstem tissues were between 1 and 0 but closer to 1. Thus forward scattering occurred in case of light-tissue interaction inside this tissue (Table 4.21)

Table 4.21

Anisotropy factors of native and coagulated brainstem tissue.

λ (nm)	Brainstem (native)	Brainstem (45°C)	Brainstem (60°C)	Brainstem (80°C)
488	0,681±0,01	0,805±0,02	0,733±0,01	0,475±0,01
514	0,75±0,02	0,822±0,01	0,728±0,01	0,495±0,01
532	0,752±0,01	0,819±0,02	0,705±0,01	0,512±0,02
633	0,739±0,02	0,844±0,01	0,756±0,01	0,543±0,01
780	0,766±0,01	0,876±0,02	0,796±0,03	0,615±0,02
810	0,836±0,02	0,884±0,02	0,802±0,02	0,622±0,01
880	0,801±0,01	0,889±0,01	0,808±0,01	0,645±0,05
905	0,824±0,03	0,898±0,03	0,819±0,03	0,66±0,03

Table 4.22

Reduced scattering coefficients of native and coagulated brainstem tissue.

λ (nm)	Brainstem (native)	Brainstem (45°C)	Brainstem (60°C)	Brainstem (80°C)
488	6,32±0,5	4,99±0,64	7,52±0,75	13,1±1,25
514	4,61±0,41	4,46±0,52	7,66±0,62	12,3±1,22
532	4,29±0,32	4,41±0,42	7,76±0,56	12±0,95
633	4,55±0,23	3,66±0,38	6,6±0,23	10,2±0,85
780	3,37±0,85	2,68±0,68	4,88±0,48	8,17±0,71
810	2,42±0,35	2,58±0,6	4,61±0,74	7,73±0,65
880	2,97±0,12	2,28±0,22	4,13±0,82	7,2±0,52
905	2,71±0,26	2,1±0,14	4,27±0,52	6,77±0,44

It was stated that, total attenuation coefficients of native cerebellar tissue tissues were less than coagulated cerebellar tissue tissues (Table 4.23). Thus, penetration depths of light through native cerebellar tissue tissues are higher than coagulated cerebellar tissue tissues at all wavelength and temperatures.

Albedo values of cerebellar tissue were between 0 and 1, but closer to 1 for all wavelengths and temperatures (Table 4.24). This means that biological cerebellar tissue tissues were turbid media and scattering of light was considerably higher than absorption for both native and coagulated brain tissues. Reduced scattering coefficients and anisotropy factors were estimated for cerebellar tissue tissues (Table 4.25, 4.26). Anisotropy factors of all cerebellar tissue tissues were between 1 and 0 but closer to 1. Thus, forward scattering occurred in case of light-tissue interaction inside this tissue (Table 4.26).

Table 4.23

Total attenuation coefficients of native and coagulated cerebellar tissue.

λ (nm)	Cerebellar tissue (native)	Cerebellar tissue (45°C)	Cerebellar tissue (60°C)	Cerebellar tissue (80°C)
488	19,86±4,21	20,59±0,82	26,4±0,33	23,09±0,5
514	17,89±1,92	19,46±0,99	26,16±1,35	22,18±0,77
532	18,14±0,7	19,46±0,31	24,47±0,74	22,77±0,45
633	18,9±0,35	19,36±1,95	22,17±0,88	18,92±0,55
780	16,2±0,95	17,54±1,25	21,06±1,54	18,43±0,87
810	16,48±1,61	17,96±0,26	21,32±0,65	12,92±0,77
880	10,39±0,65	17,62±0,45	21,44±0,84	16,51±0,66
905	15,3±0,89	17,15±0,69	20±1,52	16,37±0,33

Table 4.24

Albedo of native and coagulated cerebellar tissue.

λ (nm)	Cerebellar tissue (native)	Cerebellar tissue (45°C)	Cerebellar tissue (60°C)	Cerebellar tissue (80°C)
488	0,972±0,01	0,965±0,01	0,922±0.04	0,892±0.03
514	0,959±0,01	0,965±0,02	0,925±0,01	0,892±0,01
532	0,967±0,01	0,966±0.03	0,925±0,02	0,897±0.04
633	0,820±0,01	0,971±0,02	0,939±0,01	0,923±0,01
780	0,954±0.03	0,943±0.03	0,923±0.04	0,906±0,01
810	0,957±0,01	0,947±0,01	0,929±0,02	0,786±0,02
880	0,832±0,02	0,935±0,02	0,924±0,01	0,905±0,01
905	0,936±0,01	0,941±0,02	0,925±0.03	0,909±0.01

Table 4.25

Reduced scattering coefficients of native and coagulated cerebellar tissue.

λ (nm)	Cerebellar tissue (native)	Cerebellar tissue (45°C)	Cerebellar tissue (60°C)	Cerebellar tissue (80°C)
488	0,54±0,02	0,54±0,02	2,88±0,08	3,53±0,21
514	0,67±0,02	0,5±0,02	2,57±0.02	3,32±0,1
532	0,46	0,47±0.01	2,52±0.08	3,04±0,1
633	0,69±0.01	0,39±0,01	1,99±0.07	2,23±0,11
780	0,36±0.05	0,29±0.01	1,24±0,05	1,51±0,14
810	0,42±0,01	0,38±0,01	1,24±0,05	1,89±0,1
880	0,73±0.01	0,31±0,02	1,09±0,05	1,18±0,1
905	0,5±0.01	0,61±0,02	1,03±0,05	1,14±0,09

It was stated that, total attenuation coefficients of native frontal lobe grey matter tissues were less than coagulated frontal lobe grey matter tissues (Table 4.27). Thus, penetration depths of light through native grey matter tissues were higher than coagulated cerebellar tissue tissues at all wavelength and temperatures.

Albedo values of grey matter tissue were between 0 and 1, but closer to 1 for all wavelengths and temperatures (Table 4.28). This means that biological grey matter tissues were turbid media and scattering of light was considerably higher than absorption for both native and coagulated brain tissues. Reduced coefficients and anisotropy factors were estimated for grey matter tissues (Table 4.29, 4.30). Anisotropy factors of all grey matter tissues were between 1 and 0 but closer to 1. Thus, forward scattering occurred in case of light-tissue interaction inside this tissue (Table 4.30).

Table 4.26

Anisotropy of native and coagulated cerebellar tissue.

λ (nm)	Cerebellar tissue (native)	Cerebellar tissue (45°C)	Cerebellar tissue (60°C)	Cerebellar tissue (80°C)
488	0,972±0,01	0,971±0,01	0,881	0,828±0,03
514	0,960±0,03	0,972±0,02	0,883±0,04	0,831±0,03
532	0,973±0,01	0,974±0,01	0,888	0,847±0,01
633	0,965±0,03	0,979±0,02	0,904±0,02	0,872±0,01
780	0,976±0,01	0,981±0,03	0,936±0,02	0,909±0,03
810	0,973±0,03	0,977±0,01	0,937±0,02	0,812±0,01
880	0,914±0,02	0,98±0,03	0,944±0,02	0,92±0,03
905	0,964±0,03	0,962±0,02	0,944±0,03	0,922±0,03

Table 4.27

Total attenuation coefficients of native and coagulated grey matter tissue.

λ (nm)	Grey Matter (native)	Grey Matter (45°C)	Grey Matter (60°C)	Grey Matter (80°C)
488	18,88±0,58	22,39±4,25	24,67±1,96	24,66±0,65
514	12,44±4,65	21,57±4,96	23,92±0,85	23,91±0,58
532	17,81±1,21	20,04±3,78	24,28±0,56	23,91±0,43
633	17,25±2,02	17,29±0,96	21,74±0,75	22,29±1,52
780	11,71±0,54	13,22±1,56	20,81±0,45	21,98±1,69
810	8,4±0,26	10,06±3,15	20,12±0,38	20,57±0,75
880	10,18±0,33	12,03±2,2	20±0,33	19,57±0,81
905	9,74±0,41	10,86±1,65	20,22±0,27	19,36±0,22

It was stated that, total attenuation coefficients of native frontal lobe white matter tissues were less than coagulated frontal lobe white matter tissues except at 514-nm (Table 4.31). Total attenuation coefficient of native white matter tissue was higher than coagulated at 45°C due to high scattering coefficient. Thus, penetration depths of light through native white matter tissues were higher than coagulated white matter tissues except 514-nm

Albedo values of white matter tissue were between 0 and 1, but closer to 1 for all wavelengths and temperatures (Table 4.32). This means that biological white matter tissues were turbid media and scattering of light was considerably higher than absorption for both native and coagulated brain tissues.

Reduced coefficients and anisotropy factors were estimated for grey matter tissues (Table 4.33, 4.34). Anisotropy factors of all white matter tissues were between 1 and 0 but

closer to 1. Thus, forward scattering occurred in case of light-tissue interaction inside this tissue (Table 4.34).

Table 4.28

Albedo of native and coagulated frontal lobe grey matter tissue.

λ (nm)	Grey Matter (native)	Grey Matter (45°C)	Grey Matter (60°C)	Grey Matter (80°C)
488	0,947±0,02	0,945±0.03	0,915±0,02	0,915±0,01
514	0,876±0.03	0,937±0,02	0,918±0,01	0,919±0,02
532	0,945±0.03	0,931±0,01	0,927±0.03	0,925±0,01
633	0,958±0,01	0,915±0,01	0,943±0,01	0,954±0,02
780	0,918±0,01	0,792±0,02	0,924±0,02	0,931±0,01
810	0,929±0,01	0,725±0.03	0,924±0,02	0,933±0,02
880	0,913±0,02	0,731±0,01	0,918±0,01	0,925±0,01
905	0,902±0,01	0,677±0,01	0,92±0,01	0,928±0,01

Table 4.29

Reduced scattering coefficients of native and coagulated frontal lobe grey matter tissue.

λ (nm)	Grey Matter (native)	Grey Matter (45°C)	Grey Matter (60°C)	Grey Matter (80°C)
488	1,24±0,12	1,33±0,21	2,96±0,32	2,54±0,41
514	1,58±0,25	1,36±0,15	2,52±0,38	2,28±0,31
532	0,91±0,1	1,16±0,09	2,37±0,45	2,02±0,22
633	0,95±0,08	1,24±0,1	1,73±0,33	1,5±0,21
780	0,7±0,09	1,27±0,21	1,19±0,12	1±0,12
810	0,76±0,05	1,47±0,29	1,26±0,1	1±0,15
880	0,64±0,04	1,37±0,18	1,13±0,08	0,85±0,1
905	0,84±0,06	1,55±0,23	1,13±0,09	0,88±0,09

Table 4.30

Anisotropy factors of native and coagulated frontal lobe grey matter tissue.

λ (nm)	Grey Matter (native)	Grey Matter (45°C)	Grey Matter (60°C)	Grey Matter (80°C)
488	0,93±0,02	0,937±0,01	0,868±0,01	0,887±0,01
514	0,854±0,01	0,932±0,02	0,884±0,01	0,896±0,02
532	0,945±0,01	0,937±0,02	0,894±0,02	0,907±0,02
633	0,94±0,01	0,921±0,01	0,915±0,02	0,928±0,02
780	0,95±0,02	0,878±0,01	0,937±0,02	0,95±0,01
810	0,947±0,01	0,797±0,02	0,932±0,01	0,947±0,01
880	0,956±0,01	0,843±0,01	0,938±0,02	0,952±0,02
905	0,934±0,01	0,788±0,01	0,939±0,01	0,95±0,02

Table 4.31

Total attenuation coefficients of native and coagulated frontal lobe white matter tissue.

λ (nm)	White Matter (native)	White Matter (45°C)	White Matter (60°C)	White Matter (80°C)
488	26,96±0,78	28,75±4,29	29,4±1,45	30,93±1,01
514	29±1,95	21,69±4,45	29,39±2,28	30,17±0,51
532	24,94±0,95	25,99±0,95	30,5±0,91	29,21±0,43
633	23,15±0,86	23,82±0,62	27,82±0,29	29,82±4,41
780	23,96±2,02	25,36±0,6	25,99±1,95	26,38±0,41
810	23,28±0,98	24,15±0,71	26,7±0,73	24,67±1,15
880	19,86±0,73	24,26±0,51	25,52±1,21	25±0,88
905	21,91±1,94	26,39±0,45	26,68±0,56	25,01±0,52

Table 4.32

Albedo of native and coagulated frontal lobe white matter tissue.

λ (nm)	White Matter (native)	White Matter (45°C)	White Matter (60°C)	White Matter (80°C)
488	0,904±0,01	0,916±0,02	0,905±0,02	0,912±0.03
514	0,904±0,02	0,912±0,01	0,908±0,02	0,905±0,02
532	0,896±0.01	0,9±0,02	0,91±0,01	0,905±0.03
633	0,913±0,02	0,946±0,02	0,924±0,02	0,925±0,02
780	0,906±0.03	0,894±0,02	0,895±0,02	0,897±0,01
810	0,902±0.02	0,892±0,02	0,898±0,02	0,895±0,02
880	0,881±0.02	0,886±0,02	0,884±0,01	0,89±0,02
905	0,901±0.01	0,886±0,01	0,89±0,02	0,894±0,01

Table 4.33

Reduced scattering coefficients of native and coagulated frontal lobe white matter tissue.

λ (nm)	White Matter (native)	White Matter (45°C)	White Matter (60°C)	White Matter (80°C)
488	7,11±0,85	7,44±0,81	9,12±1,1	12,3±1,28
514	6,98±0,78	5,44±0,56	8,72±1,15	11,7±1,56
532	7,11±0,8	6,46±0,6	8,77±0,92	11,2±1,23
633	6,44±0,71	8,02±0,57	7,61±0,89	9,48±0,89
780	4,54±0,42	4,12±0,26	6,08±0,74	7,69±0,58
810	4,89±0,35	3,76±0,32	5,78±0,51	7,31±0,71
880	4,51±0,32	3,43±0,3	5,14±0,65	6,63±0,54
905	4,03±0,3	3,26±0,25	5,05±0,53	6,27±0,76

Table 4.34

Anisotropy factors of native and coagulated frontal lobe white matter tissue.

λ (nm)	White Matter (native)	White Matter (45°C)	White Matter (60°C)	White Matter (80°C)
488	0,708±0,01	0,717±0,02	0,657±0,02	0,561±0,01
514	0,708±0,02	0,725±0,01	0,673±0,03	0,576±0,01
532	0,681±0,02	0,723±0,03	0,683±0,02	0,584±0,01
633	0,695±0,01	0,644±0,02	0,703±0,01	0,658±0,02
780	0,79±0,03	0,818±0,03	0,738±0,03	0,677±0,01
810	0,76±0,02	0,825±0,02	0,758±0,02	0,669±0,02
880	0,742±0,01	0,839±0,02	0,771	0,703±0,01
905	0,795	0,849±0,03	0,787±0,02	0,72

5.   DISCUSSION

In this study, optical properties of native and coagulated lamb brain tissues within visible and near-infrared spectrum of light were estimated *in vitro*. In chapter 4, it was stated that chromophores in biological tissues such as water and hemoglobin could affect optical properties.

Generally, it was observed from the results that, absorption coefficients of native cerebellar tissue, brainstem, white matter and grey matter tissues were higher for shorter wavelengths (488-nm, 514-nm and 532-nm) related to hemoglobin absorption window [8]. It was reported in literature that as wavelength increased, absorption coefficients decreased in red region (600-700-nm) and red to NIR [8]. In this study, at 633-nm, maximum penetration depth is observed in visible light spectrum. In NIR, absorption coefficients increase due to absorption spectrum of water [8]. It was stated that due to results, absorption coefficient values were observed also higher for 810-nm, 880-nm, 905-nm due to water absorption spectrum like literature reports (Figure 4.2, 4.3, 4.4, and 4.5). These effects of water and haemoglobin on absorption of native tissues were also consistent for coagulated tissues in this study.

Concerning similarities of absorption and scattering coefficients of native brain tissues which were examined by using t-test, there were significant differences between grey matter and white matter due to their anatomic differences (Table 4.3, 4.4). White matter has water content of 72 % whereas grey mater has 82 % [28, 29]. Myelin concentration in white matter is higher than grey matter. Myelin is composed of protein and lipid. But lipid to protein ratio is high in myelin while protein content (10 %) of grey matter is higher than white matter. But there were no significant differences of absorption coefficients between native brainstem and native white matter tissues at 488nm, 514nm and 532nm (Table 4.3). These wavelengths correspond to hemoglobin absorption band, which in turn could affect absorption.

The average scattering coefficient of tissue depends on factors such as the relative refractive index between the scattering objects and their surrounding media, size and shape of the objects and densities of scatterers. Therefore, changes in wavelength-dependence of the scattering coefficient with temperature are more likely to be governed by morphological

changes. As mentioned in chapter 4, scattering coefficients decreased as wavelength increased due to increase in mie scattering and decrease in rayleigh scattering.

Before estimation of optical properties of different brain tissues, optical tissue characterization of whole blood tissue was estimated in order to measure reliability of experimental setup. Absorption coefficient values of whole blood tissue were higher at 488-nm, 514-nm, and 532-nm due to absorption band of hemoglobin which is between 400-550-nm (Table 4.1). It has even absorption peaks at 420nm and 550nm [28, 29]. After these wavelengths, at 633-nm, absorption coefficient decreased drastically. Due to low values of absorption and scattering coefficients, maximum penetration of light was observed at 633-nm within visible range (Figure 4.1). It was also found that absorption increased as wavelength increased through red to NIR. However in literature reports, as wavelength increases from red region up to NIR, absorption coefficient decreases. However, when estimated optical properties of whole blood were compared to literature reports for 488-nm in order to show accuracy of system, (Table 4.2) results were satisfactory. Scattering coefficients were different from literature report at 488-nm due to experimental setup [27]. Since literature reports were acquired using laser in experiments instead of light, scattering coefficients and related to this, total attenuation coefficients were different. However μ_a values were very close to each other.

As wavelength increases, scattering decreases due to literature reports. It was stated due to results of this study, scattering coefficients have a tendency of decreasing as wavelength increased for all tissues at all temperature values (Figure 4.6, 4.7, 4.8 and 4.9), generally. These findings may be explained by decrease in rayleigh scattering and increase in mie scattering with increase of wavelength [3] However at 810-nm for brainstem tissues which were coagulated at 45°C and 60°C, it was observed that scattering coefficients were higher than the ones at 780-nm (Table 4.8). This result can be reasonable in view of lower absorption at these temperatures and at same wavelength. It was stated that, absorption coefficients of coagulated brainstem tissues at 45°C and 60°C at 810-nm were lower than the ones at 780-nm (Table 4.7). Also it was observed from the results that optical albedos of brainstem tissues coagulated at these temperatures at 810-nm were higher than the ones at 780-nm due to low absorption at 810-nm (Table 4.20). Thus, due to low absorption at 810-nm, scattering could be higher.

As any biological tissue is coagulated, increase in temperature causes considerable brain tissue shrinkage due to loss of water in brain tissue and condensation, collagen swelling and homogenization of vessel walls. As water loss in brain tissue increases, density of chromophores and scattering imhomogenities also increases, which in turn makes tissue optically denser [4]. Thus, scattering coefficients drastically increased [3, 28]. Also scattering effects in tissues are related to their contents. In chapter 4, it was proved that there were significant differences between scattering coefficients of native and coagulated values of same tissue (Table 4.7, 4.8, 4.9, 4.10, 4.11, 4.12, 4.13 and 4.14). From the results, it was observed that scattering coefficient values of white matter tissue were higher than grey matter tissue values for all temperatures. This can be explained by higher density of myelin in white matter which increases scattering [2]. In this study, scattering coefficients of white matter tissues were higher than grey matter for both native and coagulated tissues similar to this report (Table 4.12, 4.14). However due to other literature report, as temperature increases, lipid that mostly found in white matter, undergoes a transition from an ordered gel phase to a more randomly ordered liquid phase and refractive index of lipid decreases. Related to reduction of refractive index, scattering of light also decreases [30]. In same literature report it was noted that, protein-to-lipid ratio is very important in case of scattering. So due to low protein to lipid ratio, white matter scattering coefficients should be lower than grey matter which has higher protein to lipid concentration. In same report, it was stated that for tissues in which the protein and lipid contents are comparable, the average scattering coefficient may show little change with temperature due to a cancellation of the opposing effects of protein and lipid. For example for grey matter, it is composed of 10 % protein and 9 % phospholipids. In view of this, results were found closer to this report for grey matter and white matter which have comparable lipid and protein contents. There were no significant differences concerning scattering coefficients of coagulated white matter and grey matter tissues individually (Table 4.12 and 4.14).

In this study, for white matter, as temperature increases, there were no extreme increases in scattering coefficients due to protein-lipid ratio (Table 4.14) . Literature reports also stated that, at 633-nm, reduced scattering coefficient of white matter did not change significantly over 30-80°C temperature range due to comparable protein-lipid ratio like found in this study (Table 4.33). However for grey matter, increase in reduced scattering coefficients in visible spectrum of light was higher than that of white matter for 60°C and

80°C (Table 4.29). Due to literature reports, since protein to lipid ratio in grey matter is higher than white matter, so protein denaturation effect on reduced scattering coefficient is higher than refractive index decreasing in lipid which decreases scattering [30] .

In literature, there are different researches about results about absorption coefficients after coagulation. *Roggan et al* concluded that μ_a was unchanged after coagulation [27]. However *Yaroslavsky et al* stated that μ_a increased due to thermal effects [3]. In this study, there were increases in μ_a values (Figure 5.1, 5.2, 5.3 and 5.4). Thus, results in this study were closer to reports of *Yaroslavsky et al.* For example when grey matter and cerebellar tissue are concerned, at 514nm native grey matter and cerebellar tissue absorption coefficients were higher than the ones coagulated at 45°C (Table 4.11 and 4.9). Hyperthermia begins between 43 -45°C. However in case of hyperthermia, it was stated that denaturation of macromolecules do not start. Since, there is no structural change observed at this temperature, change in μ_a at this temperature could not be same as at 60°C and 80°C. Generally results about absorption coefficients of all tissues were reasonable. Because, as temperature increases, cytoplasmic compounds of tissues such as high number of nerve cells for grey matter or axonal structures typical for white matter, changed after coagulation in response to heat-induced protein denaturation due to their thermal vulnerability [3].

As far as total attenuation coefficients of brainstem (Table 4.19) and grey matter (Table 4.27) were concerned, since scattering coefficients of coagulated tissues were considerably higher than native tissues, μ_t values were also higher. Same results were almost valid for cerebellar tissue (Table 4.23) and white matter (Table 4.31) tissues.

Related to total attenuation coefficients, penetration depths of tissues were estimated. (Figure 4.10, 4.11, 4.12 and 4.13). In these figures standard deviations was not shown because it is lower than 0.0001. Because of low total attenuation coefficient values, light can penetrates into native tissues easier than coagulated tissues. Generally penetration depth increases after 633-nm. It was stated that, hemoglobin absorption window affected penetration depth due to high absorption for 488, 514 and 532-nm. Even use of saline solution could not remove hemoglobin completely. As mentioned before, absorption coefficients in 810, 880 and 905-nm were higher than 633-nm values for all native and coagulated brain tissues due to water absorption spectrum. But decrease in scattering

coefficients at these three wavelength also higher than increase in absorption coefficients with respect to 633-nm values. Thus, lower penetration depth at 633-nm with respect to 810, 880 and 905-nm is reasonable.

6.   CONCLUSION

In this study, optical properties (μ_a, μ_s, μ_t, μ_s', τ, α, g) of native and coagulated (at 45°C, 60°C, 80°C) lamb brain tissues within visible and near-infrared spectrum of light were estimated *in vitro*. During experimental study, brainstem, cerebellar tissue, white matter and grey matter tissues of lamb brain were used. These properties were estimated due to measured data.   After experimental system was set, total transmittance, total reflectance, diffused transmittance and diffuse reflectance values of tissues were measured for both native and coagulated tissues. Data obtained from experiments were used to estimate optical properties of tissues by means of software (CAL-g3).

It is concluded that scattering coefficients of all brain tissues decreased as wavelength increases due to increase in mie scattering and decrease in rayleigh scattering. Also it was stated that as temperature of tissue increased, both absorption and scattering coefficients of tissues increased related to structural changes occur in tissues because of protein denaturation and water loss.

After estimation of optical properties, tissue similarities between native tissues for each wavelength were determined. These similarities were determined by means of different tests. Significant differences between absorption and scattering coefficients of native tissues for each wavelength were shown in different tables. In order to determine significant differences related to temperature change, anova test was applied. Both native and coagulated tissue values set as a group. While specific tissue and its coagulated values were group, only wavelengths were changed for each group. Aim of anova test is to investigate significant differences of scattering and absorption coefficients between coagulated and native tissues as temperature changes for same wavelength. As a result, significant differences were observed between coagulated and native samples of same tissues as temperature changes.

Since albedo values for native and coagulated brain tissues were between 0 and 1, all media are turbid media. It was concluded that, scattering types were forward scattering for all of native and coagulated brainstem, cerebellar tissue, grey matter and white matter tissues due to anisotropy factors.

In future studies, experimental setup used in this thesis can be developed. Ultraviolet light source can be used in order to get optical properties of tissues in UV range. Also other gratings of monochromator can be used and software can be developed in order to get whole spectrum results. Same procedure can be applied to other biological tissues.
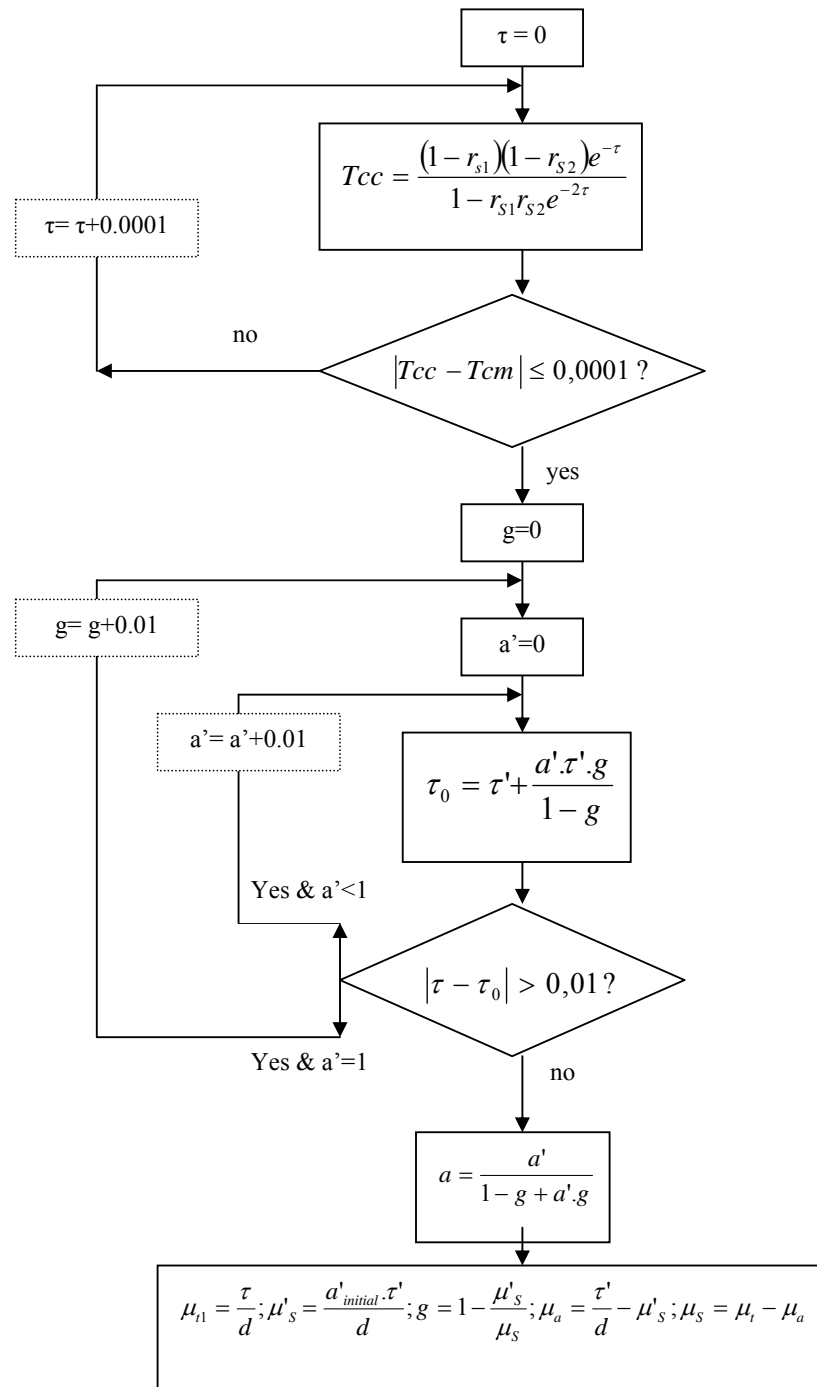
APPENDİX A: ALGORITHM OF CAL-g3

The flowchart contains the following elements:

Start box: $\tau = 0$

Loop return: $\tau = \tau + 0.0001$

Process box:
$$Tcc = \frac{(1 - r_{s1})(1 - r_{S2})e^{-\tau}}{1 - r_{S1}r_{S2}e^{-2\tau}}$$

Decision (no / yes):
$$|Tcc - Tcm| \leq 0,0001 \ ?$$

Process: $g = 0$

Loop: $g = g + 0.01$

Process: $a' = 0$

Loop: $a' = a' + 0.01$

Process box:
$$\tau_0 = \tau' + \frac{a'.\tau'.g}{1 - g}$$

Decision (Yes & a'<1 / Yes & a'=1 / no):
$$|\tau - \tau_0| > 0,01 \ ?$$

Process box:
$$a = \frac{a'}{1 - g + a'.g}$$

Final box:
$$\mu_{t1} = \frac{\tau}{d}; \mu'_S = \frac{a'_{initial}.\tau'}{d}; g = 1 - \frac{\mu'_S}{\mu_S}; \mu_a = \frac{\tau'}{d} - \mu'_S; \mu_S = \mu_t - \mu_a$$

Figure A.1 Algorithm of CAL-g3.

T_{cc} is a calculated collimated transmittance. r_{s1} and r_{s2} are specular reflection at the glass-air interface and glass-tissue interface respectively. T_{cm} is actually measured collimated transmittance. α' is the reduced albedo. α' is defined as follows:

$$a' = \begin{cases} 1 - \left(\dfrac{1 - 4.R_d - T_T}{1 - T_T} \right)^2 & \text{if } \dfrac{R_d}{1 - T_T} < 0,1 \\ \\ 1 - \dfrac{4}{9} \cdot \left(\dfrac{1 - R_d - T_T}{1 - T_T} \right)^2 & \text{if } \dfrac{R_d}{1 - T_T} \geq 0,1 \end{cases}$$

The reduced optical depth τ' is defined as follows:

$$\tau' = \frac{-\ln(T_T).\ln(0,05)}{\ln(R_T)}$$

APPENDIX B. KOTTLER'S FORMULA

When transmittance and reflectance measurements are done with the integrating sphere, the values obtained do not only refer to the tissue sample, but also to the glass slides that are on both sides of this tissue on the sample slide.

Therefore, the measured values should be corrected.   In order to do these corrections, the following Kottler formulas are used in CAL-g3 software:

$$Tt_{corrected} = \frac{\alpha.Tt_{measured}}{\alpha^2.(B.r_i + 1)^2 - r_i^2.Tt^2_{measured}}$$

$$Td_{corrected} = \frac{\alpha.Td_{measured}}{\alpha^2.(B.r_i + 1)^2 - r_i^2.Td^2_{measured}}$$

and for reflectance corrections,

$$Rt_{corrected} = \frac{1 - \sqrt{1 - 4.r_i.\left(Rt_{corrected} - r_e - r_i.Tt^2_{measured}\right)}}{2.r_i}$$

$$Rd_{corrected} = \frac{1 - \sqrt{1 - 4.r_i.\left(Rd_{corrected} - r_e - r_i.Td^2_{measured}\right)}}{2.r_i}$$

where

$$\alpha = (1 - r_i)(1 - r_e) \quad \text{and} \quad B = \frac{Rt_{measured} - r_e}{\alpha}$$

$r_i = 0,042$ and $r_e = 0,00158$ are respectively the internal and external reflections due to the glass slides.

REFERENCES

1. Stamp, J. M., " An introduction to medical lasers", *Clin. Phys. Physiol. Meas.*, Vol. 4, No. 3, pp. 267-290, Great Britain, 1983.

2. Eggert, H. R., V. Blazek, "Optical properties of human brain tissue, meninges and brain tumors in the spectral range of 200 to 900nm," *Congress of Neurological Surgeons*, vol: 21, no: 4, 1987.

3. Yaroslavsky, A. N., P. Schulze, I. V. Yaroslavsky, R. Schober, F. Ulrich, H.J. Schwarzmaier, "Optical properties of selected native and coagulated human brain tissues in vitro in the visible and near infrared spectral range," *Phys. Med. Biol.*, vol: 47, pp. 2059–2073, 2002.

4. Niemz, M. H., *Laser-Tissue Interactions*, Springer-Verlag, Berlin Heidelberg, 1996.

5. Tuchin, V., "Tissue Optics: Light scattering methods and instruments for medical diagnosis," *International Society for Optical Engineering*, Washington, USA, 2000.

6. Michael, S. B,. Edwards, M.D., J. E.Boggan, , and T. A. Fuller, "The laser in Neurosurgery," *J. Neurosurg,* vol: 59, pp. 555-566, 1983.

7. Wilson, B. C., S. L. Jacques, "Optical reflectance and transmittance of tissues: Principles and applications," *IEEE Journal of Quantum Electronics*, vol: 26, no: 12, 1990.

8. Gülsoy, M., Biophotonics, BM583 lecture notes, 2003.

9. *Scattering of light.* Available: Http://ww2010.atmos.uiuc.edu/(gh)/guides/mtr/opt/sct.

10. Cheong, W. F., S. A. Prahl, A J Welch., "A review of the optical properties of biological tissues," *IEEE Journal of Quantum Electronics*, vol: 26, no: 12, 1990.

11. Zaccanti, G., A. Taddeucci, M. Barilli, P. Bruscaglioni., F. Martelli, "Optical properties of biological tissues," *SPIE*, vol: 2389, pp. 513-521, 1995.

12. Prahl, S. A, "Light transport in tissue," PhD. thesis, University of Texas, Austin, USA, 1988.

13. Fox, S. I., *Human Physiology*, McGraw-Hill, New York, 1996.

14. *Psychology101.* Available: Http://online.morainevalley.edu/Websupported/PSY101

15. Devaux, B.C., F.X. Roux, F. Nataf, B. Turak, C. Cioloca, "High power diode lasers in Neurosurgery: Clinical Experience in 30 Cases," *Surg Neurol*, Vol.50, pp. 33-40, 1998.

16. Tabakoğlu, H. Ö., "Effects of the 980-nm diode laser versus the monopolar electrocoagulator on the rat brain," Master's thesis., Bogazici University, Istanbul, Turkey, 2003.

17. Goebel, K.R., "Fundamentals of laser science," *Acta Neurochir*, Vol.61, pp. 20-33,1994.

18. Gülsoy, M., T. Çelikel, A. Kurt, R. Canbeyli, I. Çilesiz, "980-nm wavelength diode laser application in stereotaxic laser neurosurgery in the rat," *Proc. SPIE*, Quebec, July, Vol. 3414, pp. 17-22, Canada, 1998.

19. Baggot, J., *Optical aberrations.* Available: Http://cvu.strath.ac.uk/courseware/ msc/jbaggot/aberration/aberration.html.

20. *Aspherical lenses.* Available: Http://www.canon.com/technology/p_tech/06.html

21. Francis, Y. T. S., I. C. Khoo, *Principles of Optical Engineering*, John Wiley & Sons, New York, 1990.

22. *Digikröm DK480 Monochromator/ Spectrograph User Manual* , Spectral Products, January 2003.

23. Pickering, W., S. A. Prahl, N. V. Wieringen, J. F. Beek, H. J. C. Sterenborg, M. J. C. V Gemert, "Double-integrating-sphere system for measuring the optical properties of tissue," *Appl. Opt*., no:32, pp. 399-410, 1993.

24. *Model SR540 Optical Chopper User Manual*, Stanford Research Systems, USA, 1997.

25. *Model SR510 Lock-in Amplifier User Manual* , Stanford Research Systems, USA, 1989.

26. Akarcay H. G., *Characterisation of Optical Properties of Biological Tissues*, Boğazici University, Istanbul, Turkey, 2004.

27. Sardar, D. K. and L. B. Levy,"Optical properties of whole blood," *Lasers. Med. Sci*, vol:13, pp. 106–111, 1988.

28. Roggan A., O. Minet, C. Shröder, G. Müller, "Measurements of optical tissue properties using integrating sphere technique," *Laser-Medizin-Zentrum GmbH*, pp. 6-10, D-1000 Berlin 45, 1999.

29. *Normal brain.* Available: Http://mripractice.tripod.com/mrpractice/id21.html.

30. Veronica, A., *Methods of tissue temperature measurement,* 1997. Available: http://www.medphys.ucl.ac.uk/research/borl/homepages/veronica/thesis/chapter4.pdf.